Supporting Information

Oxygenate Production from Plasma-Activated Reaction of CO_2 and Ethane

Akash N. Biswas[†,1], *Lea R. Winter*[†,1,2,*], *Björn Loenders*[†,3], *Zhenhua Xie*[4], *Annemie Bogaerts*[3,*], *Jingguang G. Chen* [1,4,*]

1. Department of Chemical Engineering, Columbia University, New York, NY 10027, USA

2. Current address: Department of Chemical and Environmental Engineering, Yale University, New Haven, CT 06520, USA

3. Department of Chemistry, University of Antwerp, B-2610 Wilrijk, Antwerp, Belgium

4. Chemistry Division, Brookhaven National Laboratory, Upton, NY 11973, USA

Corresponding authors: leawinter@yale.edu, annemie.bogaerts@uantwerpen.be, jgchen@columbia.edu

[†] These authors contributed equally.

1. Experimental Methods

1.1. Flow Reactor Experiments.

The plasma-activated reactions of CO_2 and ethane were carried out in an atmospheric-pressure steady-state flow reactor, as described previously.[1] A schematic of the U-tube reactor equipped with an external furnace is shown in Figure S1. A grounded K-type thermocouple rod (TC, 1 mm diameter) was inserted through the center of the tube and served as the ground electrode. An 8 cm-long tantalum coil was wrapped around the quartz tube and connected to the plasma generator, resulting in a 2.7 mm discharge gap (1.5 mm air gap and 1.2 mm quartz tube wall). The outlet flow was analyzed online by gas chromatography (GC, Agilent, 7890B).

The DBD plasma was powered by connecting the external power electrode to an AC plasma generator (Nanjing Suman Plasma Technology Co., Ltd, CTP-2000K). The current was adjusted in order to attain the resonant frequency for the system. During reactions, the plasma power was controlled by maintaining a frequency of 9 kHz and varying the input voltage at 6.5 kV (8.0 W), 7.3 kV (10.4 W), 8.1 kV (13.8 W), and 10.0 kV (17.9 W). The QV Lissajous method was used to calculate the plasma power.[2] Plasma measurements were taken by electrically isolating the TC from electrical ground. The TC electrode was grounded across a 10 nF capacitor in order to measure the electric charge during the reaction. A two-channel digital oscilloscope (Tektronix, TDS-210) was employed to monitor the frequency and voltage input from the power supply as well as the voltage across the capacitor.

For all experiments, a total flow rate of 15.8 mL min^{-1} consisting of 5 mL min^{-1} He, 0.8 mL min^{-1} Ar, and variable CO_2 and ethane flow rates was fed to the reactor using mass flow controllers (MFCs, Brooks Instruments). He was included in order to obtain a more uniform plasma.[3,4] Because the reaction leads to gas expansion, Ar was included as an internal volume standard to ensure the accuracy of GC calibrations. The plasma reactions took place over 7 h, with a stable product output achieved after about 200 min of the reaction.

The U-tube reactor used for steady-state flow reactor experiments consisted of MPM 214 semiconductor-grade fused quartz. The inner diameter of the quartz tube was 4 mm and the outer diameter was 6.35 mm. The U-tube reactor was surrounded by an external furnace in order to maintain the temperature at 473 K, where the controller was connected to the grounded TC in a negative feedback loop. The TC was used to directly measure the temperature within the plasma region (or in direct contact with the catalyst bed for experiments using catalyst packing). The use of the external furnace ensured that the gas temperature remained constant for different plasma powers, since the Joule heating by plasma varies with input powers, and a temperature of 473 K was well above the maximum temperature detected. The reactor outlet flow was heated to 393 K in order to avoid condensation and was analyzed online by gas chromatography equipped with PoraPLOT Q and Mol Sieve columns and a gas isolation valve. Hydrocarbon and oxygenate products were analyzed with a flame ionization detector (FID), and CO, CO_2, H_2O, and Ar were detected using a thermal conductivity detector (TCD).

Averages from the seventh to tenth GC injections (230 to 340 min) were used for steady-state data analysis. Reactant conversion, X_i, was calculated using the feed flow rate of reactant i, $F_{i,\mathrm{in}}$, and the outlet flow rate of the reactant, $F_{i,\mathrm{out}}$, as:

$$X_i = \frac{F_{i,in} - F_{i,out}}{F_{i,in}} \times 100\% \tag{S1}$$

The selectivity or product distribution S_j for a product j is given by:

$$S_j = \frac{F_{j,out}}{\sum F_{j,out}} \times 100\% \tag{S2}$$

where $\Sigma F_{j,\mathrm{out}}$ is the total flow rate of all carbonaceous species from a product j.

$RhCo_3$/MCM-41 catalysts were prepared according to the incipient wetness impregnation procedure described by Xie et al.[5] $Rh(NO_3)_3 \cdot xH_2O$, $Co(NO_3)_2 \cdot 6H_2O$, and MCM-41 were purchased from Sigma-Aldrich. Catalysts were dried at 80 °C overnight and then calcined at 290 °C for 2 h with a heating ramp rate of 0.8 °C min^{-1}. A catalyst loading of 100 mg was used, and the catalyst bed length in the U-tube reactor was 3.5 cm. All plasma-catalyst experiments were conducted at 473 K with the external furnace, as described above.

Results from flow reactor studies were used to obtain activation barrier measurements. Following the methods of Kim et al.[6] for plasma-assisted CH_4 dry reforming, the activation barriers, E_a, for CO_2 and C_2H_6 conversion in the flow reactor were evaluated by correlating the reaction rate with the specific energy input, SEI:

$$\frac{dA}{dt} = b \cdot e^{-\frac{E_a}{SEI}} \tag{S3}$$

$$SEI = \frac{P}{F} \tag{S4}$$

where dA/dt is the rate of consumption of reactant A, P is the plasma power, F is the total flow rate, and b contains pre-exponential constants. Through this modified Arrhenius equation, the exponential term is determined by the residence time of the total feed gas, as given by the total feed gas flow rate over the reaction volume, and the electron density, as given by the plasma power over the reaction volume. Essentially, the bulk reaction temperature term, RT, in the Arrhenius equation is replaced by the SEI, a parameter defined by both the plasma power and total feed gas flow rate. Linearization of Equation S3 enables estimation of E_a based on measuring the reaction rate with respect to plasma power at a constant flow rate:

$$\ln\left(\frac{dA}{dt}\right) = -E_a F \frac{1}{P} + b \tag{S5}$$

1.2. FTIR Batch Reactor Experiments

In situ spectroscopic measurements were carried out in a custom high vacuum batch reactor, as described previously.[1] The chamber was modified with two custom-designed high voltage electrical feedthroughs (MDC Vacuum Products) and insulated parallel-plate copper electrodes of 7.6 mm diameter covered by a 1.5 mm thick quartz plate. The electrodes were mounted on single-axis motion manipulators in horizontal alignment and electrically connected to the plasma generator and ground, respectively. The plasma power was measured as described above using the QV Lissajous method.

The batch reactor was equipped with a Thermo Nicolet Nexus 470 spectrometer and a mercury cadmium telluride (MCT-A) detector. Reactants were prepared by dosing 600.0 Torr He, 75.0 Torr CO_2, and 75.0 Torr C_2H_6 into the vacuum chamber, for a total pressure of 750.0 Torr. The high He dilution ratio was required in order to enable sufficiently high plasma power without inducing arcing to the metallic chamber walls and in order to improve the spectrometer signal-to-noise ratio, while enabling operation at atmospheric pressure in order to match more closely the conditions of the flow reactor. The plasma was operated at 9.5 kV and 8.5 kHz for 3 h. FTIR spectra of the gas phase were recorded as a function of time with one spectrum collected every 30 s. Experiments using $^{13}CO_2$ isotope gas ($^{13}CO_2$, Sigma-Aldrich 99 atom% ^{13}C, <3 atom% ^{18}O) were carried out as described previously.[7]

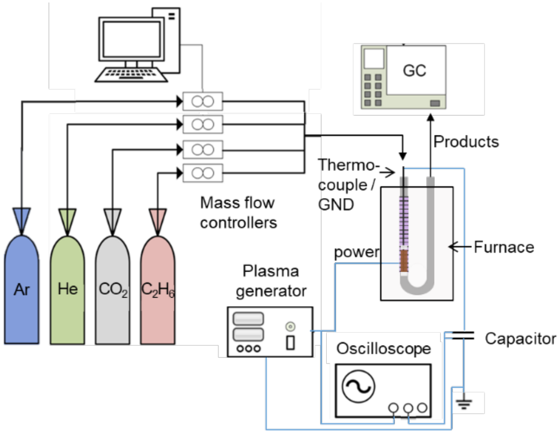

Figure S1. U-tube flow reactor setup with external furnace heating. Gases were flowed into the quartz reactor and the product stream was analyzed using gas chromatography. The plasma power was monitored by generating a QV Lissajous figure with the voltage input from the plasma generator and the voltage across an external capacitor connected between the ground electrode and electrical ground.

2. Experimental Results

2.1. Plasma Flow Reactor Studies.

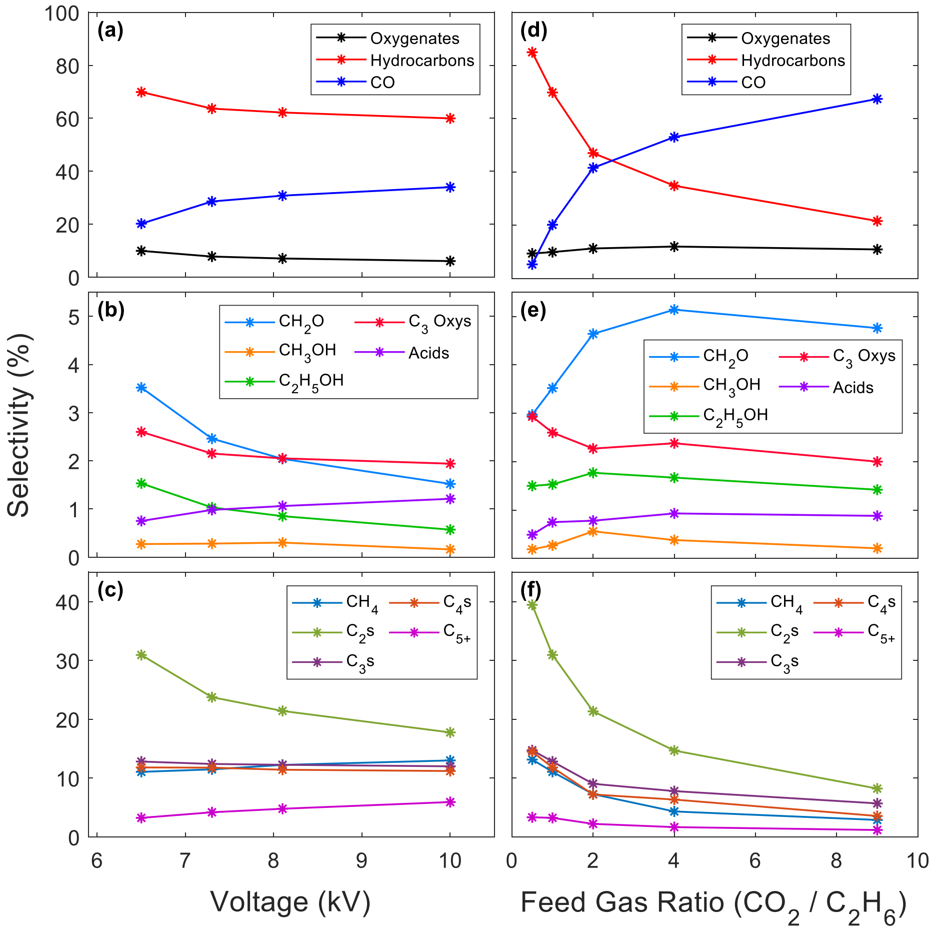

Figure S2. (a–c) Plasma power effects for 1:1 CO_2 to C_2H_6 feed gas ratio at ambient pressure and 473 K. (d–f) Feed gas ratio effects at 6.5 kV at ambient pressure and 473 K. Selectivity of CO, total hydrocarbons, and total oxygenates (top row), selectivity of oxygenate products (middle row), and selectivity of hydrocarbon products (bottom row) are shown. 'C_3 Oxys' include 1-propanol, 2-propanol, and propanal; 'Acids' include acetic acid and propanoic acid. 'C_2s' include acetylene and ethylene; 'C_3s', 'C_4s', and 'C_5s' include higher-order hydrocarbons. Values are averaged over four GC injections measured at steady state.

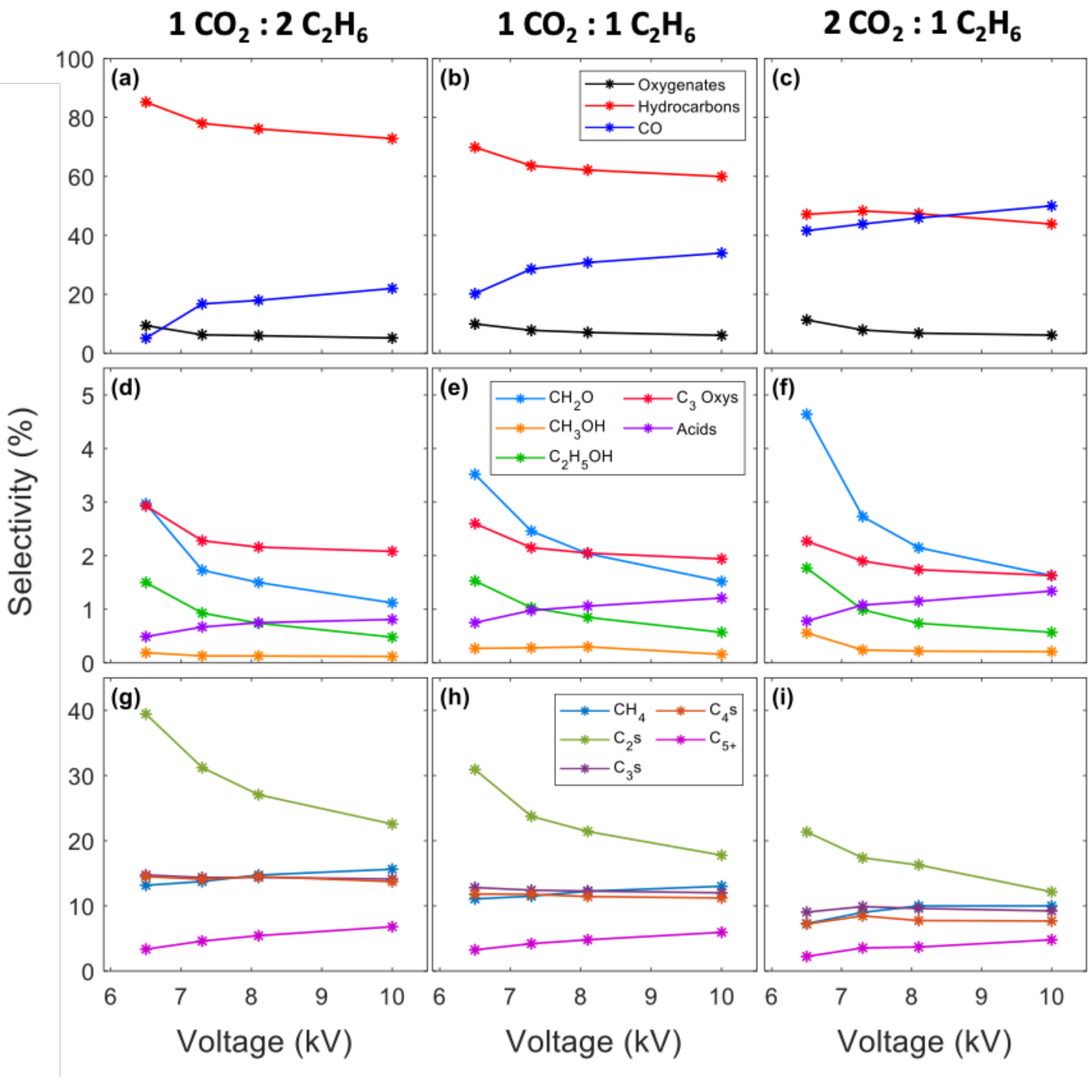

Figure S3. Plasma power effects for different CO_2 to C_2H_6 feed gas ratios under ambient pressure and 473 K. Selectivity of CO, hydrocarbons, and oxygenates for (a) 1:2, (b) 1:1, and (c) 2:1 CO_2 to C_2H_6 feed gas ratios. Selectivity of oxygenate products for (d) 1:2, (e) 1:1, and (f) 2:1 CO_2 to C_2H_6 feed gas ratios. "C_3 Oxys" include 1-propanol, 2-propanol, and propanal; 'Acids' include acetic acid and propanoic acid. Selectivity of hydrocarbon products for (g) 1:2, (h) 1:1, and (i) 2:1 CO_2 to C_2H_6 feed gas ratios. 'C_2s' include acetylene and ethylene; 'C_3s', 'C_4s', and 'C_5s' include higher-order hydrocarbons. Values are averaged over four GC injections measured at steady state.

Table S1. Conversion, carbon and oxygen balance, and overall selectivities and yields for varied plasma powers and feed gas ratios. Selectivities are calculated as a fraction of total carbonaceous species produced according to Equation S2. Yields are calculated with respect to ethane conversion. Values are averaged over four injections measured at steady state.

Feed Gas Ratio	**Voltage**	X_{CO2}	X_{C2H6}	**Carbon Balance**	**Oxygen Balance**	**CO Selectivity**	**Tot. Oxy Selectivity**	**Tot. HC Selectivity**	**Tot. Oxy Yield**	**Tot. HC Yield**
1 CO_2 : 2 C_2H_6	6.5 kV	0.9%	2.9%	100.0%	100.0%	5.4%	9.4%	85.2%	0.3%	2.5%
	7.3 kV	1.9%	6.6%	99.9%	100.3%	16.7%	6.3%	77.0%	0.4%	4.9%
	8.1 kV	3.9%	9.4%	99.3%	98.9%	18.0%	5.9%	76.1%	0.6%	7.2%
	10.0 kV	6.0%	17.1%	99.4%	99.7%	22.0%	5.1%	72.8%	0.9%	12.5%
1 CO_2 : 1 C_2H_6	6.5 kV	1.6%	5.5%	99.3%	99.6%	20.2%	9.9%	69.9%	0.5%	3.8%
	7.3 kV	2.0%	8.0%	100.1%	100.2%	28.6%	7.8%	63.6%	0.6%	5.1%
	8.1 kV	3.0%	12.4%	99.6%	100.4%	30.8%	7.1%	62.2%	0.9%	7.7%
	10.0 kV	6.2%	20.4%	98.9%	99.5%	34.0%	6.1%	60.0%	1.2%	12.2%
2 CO_2 : 1 C_2H_6	6.5 kV	0.6%	5.3%	100.5%	100.8%	41.6%	11.3%	47.1%	0.6%	2.5%
	7.3 kV	2.8%	11.9%	99.4%	99.6%	43,8%	7.9%	48.3%	0.9%	5.8%
	8.1 kV	3.5%	16.6%	99.6%	100.0%	45.9%	6.8%	47.3%	1.1%	7.8%
	10.0 kV	6.7%	27.9%	98.6%	99.5%	50.0%	6.1%	43.9%	1.7%	12.2%
4 CO_2 : 1 C_2H_6	6.5 kV	2.7%	13.1%	96.6%	98.6%	53.1%	12.0%	34.9%	1.6%	4.6%
9 CO_2 : 1 C_2H_6	6.5 kV	1.8%	13.9%	98.8%	99.7%	67.5%	10.9%	21.6%	1.5%	3.0%

Table S2. Conversion, carbon and oxygen balance, and overall selectivities and yields for varied plasma powers and feed gas ratios. Selectivities are calculated as a fraction of total carbonaceous species produced according to Equation S2. Yields are calculated with respect to ethane conversion. Values are averaged over four injections measured at steady state.

Feed Gas Ratio	Voltage	HCHO	MeOH	EtOH	1-PrOH	2-PrOH	Propanal	Acetic Acid	Propanoic Acid	Other Oxy
1 CO_2 : 2 C_2H_6	6.5 kV	3.0%	0.2%	1.5%	0.9%	1.4%	0.6%	0.3%	0.1%	1.3%
	7.3 kV	1.7%	0.1%	0.9%	0.5%	1.1%	0.5%	0.4%	0.2%	0.9%
	8.1 kV	1.5%	0.1%	0.7%	0.5%	1.2%	0.4%	0.5%	0.2%	0.8%
	10.0 kV	1.1%	0.1%	0.5%	0.3%	1.3%	0.2%	0.5%	0.3%	0.7%
1 CO_2 : 1 C_2H_6	6.5 kV	3.5%	0.3%	1.5%	0.8%	1.1%	0.7%	0.5%	0.2%	1.3%
	7.3 kV	2.5%	0.3%	1.0%	0.5%	1.0%	0.6%	0.6%	0.3%	1.0%
	8.1 kV	2.0%	0.3%	0.9%	0.5%	1.0%	0.6%	0.7%	0.3%	0.8%
	10.0 kV	1.5%	0.2%	0.6%	0.4%	1.0%	0.5%	0.8%	0.4%	0.7%
2 CO_2 : 1 C_2H_6	6.5 kV	4.6%	0.6%	1.8%	0.7%	0.8%	0.8%	0.5%	0.2%	1.3%
	7.3 kV	2.7%	0.2%	1.0%	0.5%	0.7%	0.7%	0.7%	0.3%	1.1%
	8.1 kV	2.1%	0.2%	0.7%	0.4%	0.7%	0.6%	0.7%	0.4%	1.0%
	10.0 kV	1.6%	0.2%	0.6%	0.4%	0.7%	0.5%	0.8%	0.5%	0.8%
4 CO_2 : 1 C_2H_6	6.5 kV	5.1%	0.4%	1.7%	0.8%	0.6%	1.0%	0.6%	0.3%	1.2%
9 CO_2 : 1 C_2H_6	6.5 kV	4.8%	0.2%	1.4%	0.7%	0.5%	0.9%	0.5%	0.3%	1.6%

Table S3. Selectivities of hydrocarbon products for varied plasma powers and feed gas ratios. Selectivities are calculated as a fraction of total carbonaceous species produced according to Equation S2. Values are averaged over four injections measured at steady state.

Feed Gas Ratio	Voltage	CH_4	C_2	C_3	C_4	C_{5+}
1 CO_2 : 2 C_2H_6	6.5 kV	13.2%	39.5%	14.7%	14.5%	3.4%
	7.3 kV	13.7%	30.2%	14.4%	14.1%	4.6%
	8.1 kV	14.7%	27.1%	14.4%	14.5%	5.4%
	10.0 kV	15.6%	22.6%	14.1%	13.7%	6.8%
1 CO_2 : 1 C_2H_6	6.5 kV	11.1%	30.9%	12.8%	11.8%	3.3%
	7.3 kV	11.5%	23.8%	12.4%	11.8%	4.2%
	8.1 kV	12.3%	21.4%	12.3%	11.4%	4.8%
	10.0 kV	13.0%	17.8%	12.0%	11.2%	5.9%
2 CO_2 : 1 C_2H_6	6.5 kV	7.3%	21.3%	9.0%	7.2%	2.2%
	7.3 kV	9.0%	17.4%	9.9%	8.5%	3.6%
	8.1 kV	10.0%	16.3%	9.6%	7.8%	3.7%
	10.0 kV	10.0%	12.1%	9.2%	7.7%	4.8%
4 CO_2 : 1 C_2H_6	6.5 kV	4.3%	14.7%	7.8%	6.4%	1.7%
9 CO_2 : 1 C_2H_6	6.5 kV	2.9%	8.2%	5.7%	3.6%	1.2%

2.2. Effects of $RhCo_3$/MCM-41 Catalyst.

$RhCo_3$/MCM-41 was recently shown to be an effective heterogeneous hydroformylation catalyst, converting ethylene and synthesis gas to C_3 oxygenates (propanol and propanal) at 473 K.[5] Since C_2H_4 and CO were detected in the $CO_2 + C_2H_6$ plasma reaction and significant amounts of H_2 likely were produced as well,[8,9] the $RhCo_3$/MCM-41 catalyst was considered to be a potential candidate to enhance the production of C_3 oxygenates. The effects of the catalyst on the plasma reaction were evaluated using two different plasma-catalyst configurations: the catalyst was placed inside the plasma zone (in-plasma catalysis, IPC) as well as downstream of the plasma zone (post-plasma catalysis, PPC). Evidently, IPC and PPC configurations should facilitate interactions of the catalyst bed with shorter-lived and longer-lived plasma-activated species, respectively. The IPC configuration also can modify both the catalyst properties due to direct plasma irradiation as well as the plasma electrical properties due to packing catalyst materials in the plasma.[10]

Figure S4 shows the effects of the $RhCo_3$/MCM-41 catalyst compared with plasma only experiments. For these experiments, CO_2 and C_2H_6 were fed in a 2:1 ratio and the voltage was maintained at 10.0 kV. As shown in Figure S4a, the oxygenate selectivity was enhanced for both IPC and PPC configurations between about 50 to 200 min of the experiment. The total oxygenate fraction for the PPC and IPC reactions reached up to 7.0% and 7.6%, respectively, within the first 100 min of the reaction, while the oxygenate fraction for the plasma only reaction remained stable at about 6%. At longer time on stream, the oxygenate selectivity for both PPC and IPC reactions stabilized at a value slightly higher than that of the plasma only experiment.

Figure S4b shows a depletion in C_2H_2 production for the PPC and IPC studies in the first 200 min of the experiments, with no C_2H_2 production for the first 50 and 100 min for PPC and IPC experiments, respectively, which corresponded to the timescale of increased oxygenate production. Interestingly, however, the amount of C_2H_4 remained relatively constant among the plasma only, PPC, and IPC experiments over this timescale (Figure S5a), suggesting that the hydroformylation reaction, which should consume C_2H_4 to make C_3 oxygenates, was not enhanced in the presence of the $RhCo_3$/MCM-41 catalyst. This is further supported by the similar C_3 oxygenate yields for catalyst and plasma only experiments shown in Figure S4a. Instead, the catalyst appeared to promote a competing reaction pathway that favored oxygenate formation as opposed to the ethane/ethylene dehydrogenation pathway to acetylene that occurred in the absence of the catalyst. In particular, the IPC configuration mainly enhanced formaldehyde production (Figure S5b) and the PPC configuration enhanced acid production (Figure S5c), illustrating that the placement of the catalyst with respect to the plasma region can alter the reaction mechanism and overall product distribution. Similar trends were also observed for a 1:2 CO_2 to C_2H_6 feed gas ratio, as shown in Figure S6. In Figure S7, a similar phenomenon is also demonstrated at a different plasma voltage (7.3 kV). Comparison to a blank MCM-41 experiment enabled decoupling of the effects of the $RhCo_3$ catalytic activity and surface area of the packing material, where a change in product selectivity was not observed with the blank MCM-41 packing. These results highlight the importance of dynamic changes that can occur during plasma catalysis reactions, where the effects of the catalyst can change over the course of the reaction and may depend upon the timescale of the reaction.

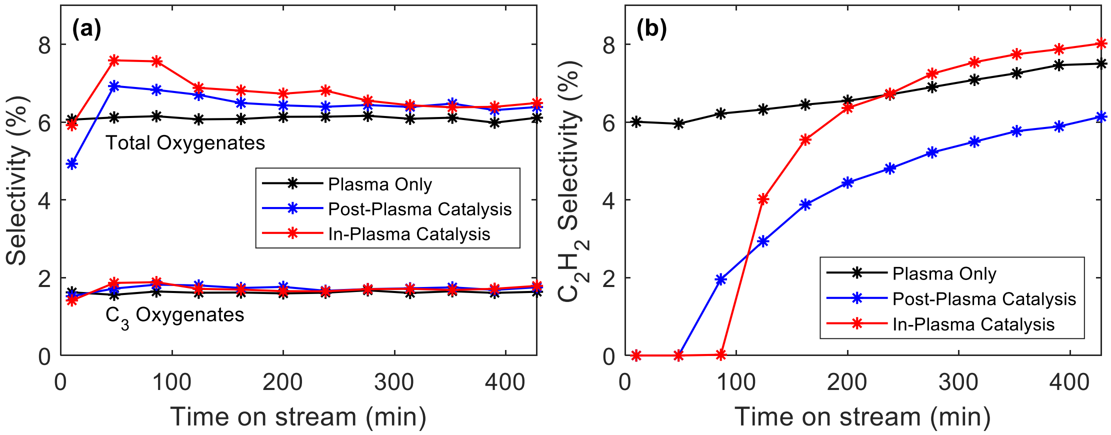

Figure S4. $RhCo_3$/MCM-41 catalyst effects for a 2:1 CO_2 to C_2H_6 feed gas ratio at 10.0 kV for experiments with plasma only/no catalyst, post-plasma catalysis, and in-plasma catalysis. (a) Selectivity of total oxygenates and C_3 oxygenates (1-propanol, 2-propanol, and propanal) following time on stream. (b) C_2H_2 selectivity following time on stream.

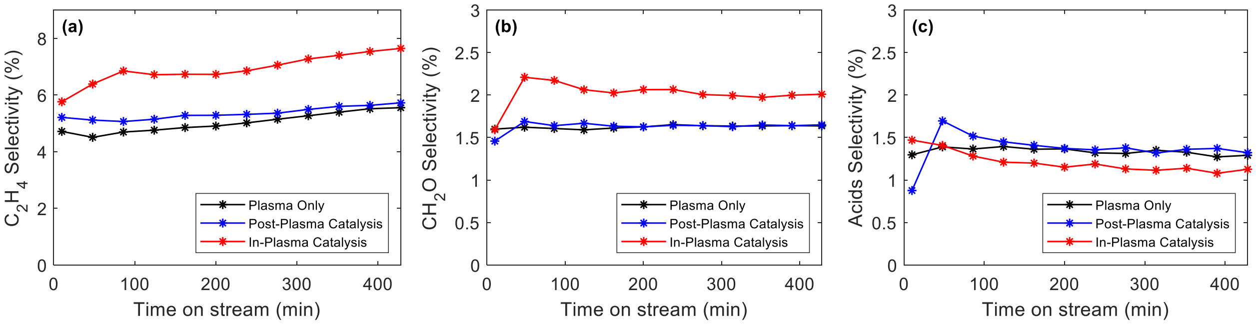

Figure S5. RhCo$_3$/MCM-41 catalyst effects for a 2:1 CO_2 to C_2H_6 feed gas ratio at 10.0 kV. Selectivity of (a) C_2H_4, (b) CH_2O, and (c) acids following time on stream.

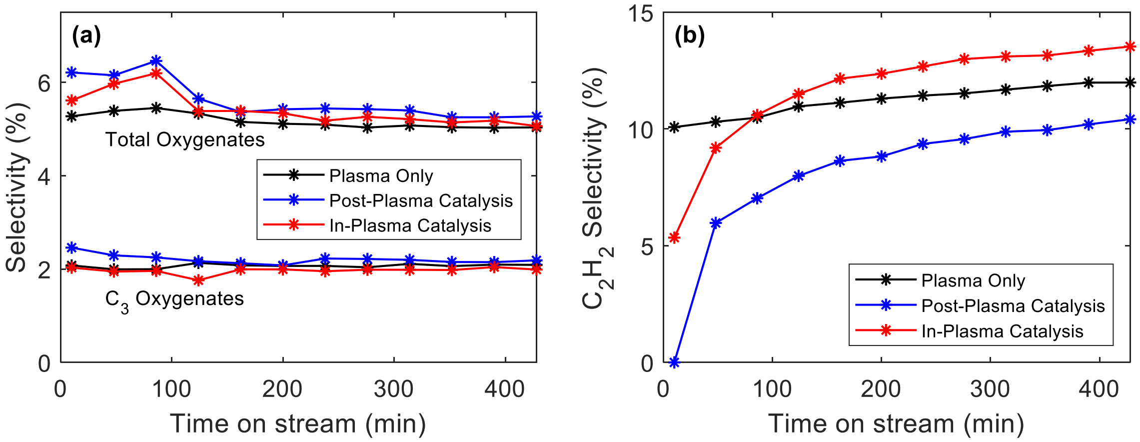

Figure S6. $RhCo_3$/MCM-41 catalyst effects for a 1:2 CO_2 to C_2H_6 feed gas ratio at 10.0 kV. (a) Selectivity of total oxygenates and C_3 oxygenates (1-propanol, 2-propanol, and propanal) following time on stream. (b) C_2H_2 selectivity following time on stream.

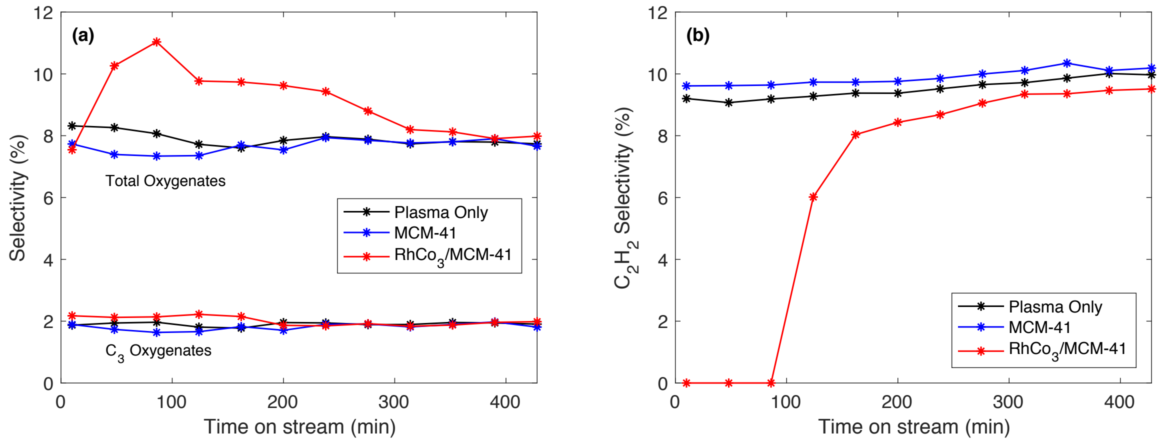

Figure S7. $RhCo_3$/MCM-41 catalyst effects for a 2:1 CO_2 to C_2H_6 feed gas ratio at 7.3 kV in comparison with plasma only and MCM-41 experiments. (a) Selectivity of total oxygenates and C_3 oxygenates (1-propanol, 2-propanol, and propanal) following time on stream. (b) C_2H_2 selectivity following time on stream.

3. Computational Methods

The numerical simulations were executed using the 0D plasma chemical kinetics solver ZDPlasKin.[11] This solver calculated the number densities n_i of the different species i as a function of time, by solving the corresponding continuity equations:

$$\frac{dn_i}{dt} = \sum_{j=1}^{j_{max}} \left(a_{i,j}^{P} - a_{i,j}^{R}\right) r_j \tag{S6}$$

where $a^{P}_{i,j}$ and $a^{R}_{i,j}$ are the stoichiometric coefficients of species i in reaction j for the products and reactants, respectively. The reaction rate r_j of reaction j was calculated from the number densities n_i of the reactants and the corresponding stoichiometric coefficients $a^{R}_{i,j}$:

$$r_j = k_j \prod\nolimits_i n_i^{a_{i,j}^{R}} \tag{S7}$$

where k_j is the rate coefficient of reaction j. The rate coefficients were taken from literature or, in the case of electron impact reactions, were calculated from the electron impact cross sections and the electron energy distribution function through BOLSIG+,[12] a numerical solver for the steady-state Boltzmann equation for electrons.

To simulate the DBD plasma, the 0D DBD model developed by van ‘t Veer et al.[13,14] was used, which was developed specifically for use in combination with the ZDPlasKin solver. In this model, the DBD reactor is treated as a plug flow reactor, meaning that the species densities only change in the axial direction and are constant along the radial dimension. Since each point along the axial dimension matches with a certain residence time, the model is solved as a function of time, i.e., without real spatial dimensions, hence the 0D model. However, because this time dependence is translated into a spatial dependence (along the axial direction) in the plug flow reactor, by means of the gas velocity, this model is also called a “quasi-1D model”. Because a DBD plasma in CO_2/C_2H_6 mixtures is filamentary, the gas molecules experience these filaments when traveling through the DBD reactor. The model simulates these filaments or microdischarges in the DBD plasma by applying periodic triangular pulses in power density. These pulses are thus characterized by a high power density and are followed by longer periods with a lower (and constant) power density, referred to as the afterglows. As such, the experimentally measured plasma power is divided over the different pulses and afterglows. For a more detailed description of the model, we refer to van ‘t Veer et al.[13,14]

The model parameters, such as the plasma power, gas temperature, applied frequency, reactor volume, and total gas flow rate, were taken to be the same as in the flow reactor experiments. Simulations were performed for a 1:1 CO_2 to C_2H_6 feed gas ratio at atmospheric pressure. Although experiments were performed in mixtures of $CO_2/C_2H_6/He$, the model only considered CO_2 and C_2H_6. He is an inert gas and is not expected to participate in the chemical reactions. He could only contribute by Penning ionization (i.e., reactions of metastable excited He atoms or dimers, causing ionization of CO_2 or C_2H_6, or other molecules) and charge transfer (i.e., reaction of He^+ or He^{2+} ions, again causing ionization), but this would not significantly affect the results since ion chemistry is typically of lower importance in DBD plasma. Therefore, our model of CO_2/C_2H_6 plasma can provide a good picture of the underlying chemistry.

Table S4 specifies the list of species included in the model. The chemistry set used for the plasma chemical kinetics modeling was compiled from reactions used in earlier modeling studies[15–18] and further extended with various neutral-neutral, ion-ion, ion-neutral, and electron-ion reactions. In addition, some electron impact cross sections and reaction rate coefficients were revised. Table S5 shows the electron impact reactions for which the cross sections have been revised. Based on the work of Morillo-Candas et al.,[19] the cross sections of CO_2 electron impact dissociation from Polak and Slovetsky[20] were used, instead of the Phelps cross sections[21] that were used in earlier modeling studies.[15–18] The cross sections for electron impact dissociation of C_2H_6 and C_3H_8 derived theoretically by Janev and Reiter[22] were found to systematically overestimate the destruction of these species. It is important to note that much of the data required to calculate these cross sections, including the threshold energies of the different dissociation channels, were unavailable and as such Janev and Reiter had to rely on estimates.[22] However, we obtained a relatively good agreement with the experimental results when using the cross section for electronic excitation of C_2H_6, C_2H_4, C_3H_8, and C_3H_6 from the LXCat database[23–25] and assuming the corresponding excited states dissociate according to the branching ratios reported in Table S5. These branching ratios were chosen so that the relative importance of the different dissociation channels at high electron energies was similar to the asymptotic branching ratios estimated by Janev and Reiter,[22] while also taking into account that the excited states can only dissociate via dissociation channels with a reaction enthalpy that is lower than the excitation threshold. Table S6 lists the reactions used to expand the chemistry set with respect to previous modeling studies,[15–18] as well as the reactions for which different rate coefficients were used.

As the exact microdischarge duration and number of microdischarge pulses per half cycle of the applied power are not known, values similar to those reported in literature for a CO_2 plasma were used as an approximation.[26] The microdischarge duration was set to 15.6 ns and the number of microdischarges per half cycle was varied from 200 to 447. The number of microdischarges was assumed to increase linearly with plasma power, as higher plasma powers have been reported to result in more microdischarges per half cycle.[26] Furthermore, a so-called power distribution factor (between the high-power microdischarge pulses and the low-power afterglows in between them) of 0.3 was assumed, which lies in the range of 0.1-1 recommended by van ‘t Veer et al.[13] The microdischarge volume was estimated to be 0.047 mm^3, assuming a cylindrical shape with a length equal to the air gap between the electrodes (1.5 mm) and a filament diameter of 0.2 mm, based on Bogaerts et al.[27] Using these parameters, the minimum and maximum power densities, as well as the effective period over which the molecules are exposed to pulses, were calculated by the model (Table S7).

Table S4. List of the species included in the model.

Elements	Molecules	Radicals	Ions	Excited species
H	H_2	H	H^+, H^-, H_2^+, H_3^+	
C		C, C_2	C^+, C_2^+	
O	O_2, O_3	O	O^+, O^-, O_2^+, O_2^-, O_3^-, O_4^+, O_4^-	$O_2(E_1\text{-}E_2)$
C, H	CH_4, C_2H_2, C_2H_4, C_2H_6, C_3H_6, C_3H_8, C_4H_8, C_4H_{10}	CH, CH_2, CH_3, C_2H, C_2H_3, C_2H_5, C_3H_5, C_3H_7, C_4H_9	CH^+, CH_2^+, CH_2^-, CH_3^+, CH_4^+, CH_5^+, C_2H^+, $C_2H_2^+$, $C_2H_3^+$, $C_2H_4^+$, $C_2H_5^+$, $C_2H_6^+$	
C, O	CO, CO_2	C_2O	CO^+, CO_2^+, CO_3^-, CO_4^-, $C_2O_2^+$, $C_2O_3^+$, $C_2O_4^+$	$CO(E_1\text{-}E_4)$, $CO_2(V_a\text{-}V_d)$, $CO_2(V_1\text{-}V_{21})$
H, O	H_2O, H_2O_2	OH, HO_2	OH^+, OH^-, H_2O^+, H_3O^+	
C, H, O	CH_2O, HCOOH, CH_3OH, CH_3OOH, CH_2CO, CH_3CHO, C_2H_5OH, C_2H_5OOH, C_2H_5CHO, C_3H_7OH	CHO, CH_3O, CH_3O_2, CH_2OH, $HOCH_2O$, COOH, HCOO, CH_3CHOH, CH_3CO, C_2H_5O, $C_2H_5O_2$, C_2HO, C_2H_5CO, C_3H_7O, $C_3H_7O_2$	CHO^+	

Table S5. Overview of the electron impact processes for which the cross sections have been revised. For the electron impact dissociation reactions of C_2H_6, C_2H_4, C_3H_8, and C_3H_6, the cross sections for excitation to the indicated electronically excited states were used and the excited states were assumed to dissociate according to the indicated branching ratios.

Reaction	**Ref.**
$CO_2 + e^- \rightarrow CO + O + e^-$	20
$CO_2 + e^- \rightarrow CO(E_1) + O + e^-$	20

Reaction	**Branching Ratio**	**From excited state**	**Ref.**
$C_2H_6 + e^- \rightarrow C_2H_4 + H_2 + e^-$	0.46	$C_2H_6(E_1)$, $C_2H_6(E_2)$	23,28
$C_2H_6 + e^- \rightarrow C_2H_5 + H + e^-$	0.24	$C_2H_6(E_1)$, $C_2H_6(E_2)$	23,28
$C_2H_6 + e^- \rightarrow C_2H_2 + 2H_2 + e^-$	0.11	$C_2H_6(E_1)$, $C_2H_6(E_2)$	23,28
$C_2H_6 + e^- \rightarrow CH_3 + CH_3 + e^-$	0.08	$C_2H_6(E_1)$, $C_2H_6(E_2)$	23,28
$C_2H_6 + e^- \rightarrow CH_4 + CH_2 + e^-$	0.07	$C_2H_6(E_1)$, $C_2H_6(E_2)$	23,28
$C_2H_6 + e^- \rightarrow C_2H_3 + H_2 + H + e^-$	0.04	$C_2H_6(E_1)$, $C_2H_6(E_2)$	23,28
$C_2H_4 + e^- \rightarrow C_2H_2 + H_2 + e^-$	1.00	$C_2H_4(E_1)$	23,29
$C_2H_4 + e^- \rightarrow C_2H_2 + H_2 + e^-$	0.30	$C_2H_4(E_2)$	23,29
$C_2H_4 + e^- \rightarrow C_2H_3 + H_2 + e^-$	0.40	$C_2H_4(E_2)$	23,29
$C_2H_4 + e^- \rightarrow C_2H_2 + 2H + e^-$	0.20	$C_2H_4(E_2)$	23,29
$C_2H_4 + e^- \rightarrow CH_4 + C + e^-$	0.10	$C_2H_4(E_2)$	23,29
$C_2H_4 + e^- \rightarrow C_2H + H_2 + H + e^-$	0.40	$C_2H_4(E_3)$	23,29
$C_2H_4 + e^- \rightarrow CH_3 + CH + e^-$	0.30	$C_2H_4(E_3)$	23,29
$C_2H_4 + e^- \rightarrow 2CH_2 + e^-$	0.30	$C_2H_4(E_3)$	23,29
$C_3H_8 + e^- \rightarrow C_3H_6 + H_2 + e^-$	0.34	$C_3H_8(E_1)$, $C_3H_8(E_2)$	24
$C_3H_8 + e^- \rightarrow C_2H_4 + CH_4 + e^-$	0.30	$C_3H_8(E_1)$, $C_3H_8(E_2)$	24
$C_3H_8 + e^- \rightarrow C_3H_7 + H + e^-$	0.22	$C_3H_8(E_1)$, $C_3H_8(E_2)$	24
$C_3H_8 + e^- \rightarrow C_2H_5 + CH_3 + e^-$	0.04	$C_3H_8(E_1)$, $C_3H_8(E_2)$	24
$C_3H_8 + e^- \rightarrow C_2H_6 + CH_2 + e^-$	0.03	$C_3H_8(E_1)$, $C_3H_8(E_2)$	24
$C_3H_6 + e^- \rightarrow C_2H_2 + CH_4 + e^-$	0.42	$C_3H_6(E_1)$	25,30
$C_3H_6 + e^- \rightarrow C_2H_2 + CH_4 + e^-$	0.22	$C_3H_6(E_2)$	25,30
$C_3H_6 + e^- \rightarrow C_3H_5 + H + e^-$	0.25	$C_3H_6(E_2)$	25,30
$C_3H_6 + e^- \rightarrow C_2H_4 + CH_2 + e^-$	0.06	$C_3H_6(E_2)$	25,30
$C_3H_6 + e^- \rightarrow C_2H_3 + CH_3 + e^-$	0.06	$C_3H_6(E_2)$	25,30

Table S6. Overview of the neutral-neutral, ion-ion, ion-neutral, and electron-ion reactions that were added to the chemistry set or for which different rate coefficients were used compared to earlier modeling studies.[15–18] For each reaction, we list the corresponding rate coefficients and the references from which these were adopted. The units of the rate coefficients are in s^{-1} and $cm^3\ s^{-1}$ for first and second order reactions, respectively. In the expressions of the rate constants T_g denotes the gas temperature in K, T_e denotes the average electron temperature in K, and R denotes the ideal gas constant in J $mole^{-1}$ K^{-1}.

Neutral-neutral reactions

Reaction	Rate coefficient	Ref.
$C_2H_4 + O \rightarrow C_2H_3 + OH$	$1.33 \times 10^{-12} \left(\frac{T_g}{298}\right)^{1.91} exp\left(\frac{-1.56 \times 10^4}{RT_g}\right)$	31
$C_2H_4 + O \rightarrow CHO + CH_3$	$1.50 \times 10^{-12} \left(\frac{T_g}{298}\right)^{1.55} exp\left(\frac{-1.788 \times 10^3}{RT_g}\right)$	32
$C_2H_4 + O \rightarrow CH_3CO + H$	$9.11 \times 10^{-13} \left(\frac{T_g}{298}\right)^{-0.48} exp\left(\frac{-8.192 \times 10^3}{RT_g}\right)$	33
$C_2H_4 + O \rightarrow CH_2O + CH_2$	$8.08 \times 10^{-13} \left(\frac{T_g}{298}\right)^{1.99} exp\left(\frac{-1.20 \times 10^4}{RT_g}\right)$	33
$C_2H_4 + O \rightarrow CH_2CO + H_2$	3.82×10^{-14}	34
$C_2H_4 + O_2 \rightarrow C_2H_3 + HO_2$	$7.01 \times 10^{-11} exp\left(\frac{-2.41 \times 10^5}{RT_g}\right)$	32
$C_2H_4 + OH \rightarrow C_2H_3 + H_2O$	$2.29 \times 10^{-13} \left(\frac{T_g}{298}\right)^{2.74} exp\left(\frac{-9.271 \times 10^3}{RT_g}\right)$	35
$C_2H_4 + H \rightarrow C_2H_5$	$1.25 \times 10^{-11} \left(\frac{T_g}{298}\right)^{1.07} exp\left(\frac{-6.067 \times 10^3}{RT_g}\right)$	36
$C_2H_4 \rightarrow C_2H_3 + H$	$2.0 \times 10^{16} exp\left(\frac{-4.61 \times 10^5}{RT_g}\right)$	37
$C_2H_4 \rightarrow C_2H_2 + H_2$	$9.75 \times 10^{13} \left(\frac{T_g}{298}\right)^{0.44} exp\left(\frac{-3.72 \times 10^5}{RT_g}\right)$	32
$CH_3 + C_2H_5 \rightarrow C_3H_8$	5.60×10^{-11}	38
$CH_3 + C_2H_5 \rightarrow C_2H_4 + CH_4$	$1.88 \times 10^{-12} \left(\frac{T_g}{298}\right)^{-0.50}$	32
$C_2H_5 + C_2H_3 \rightarrow C_2H_6 + C_2H_2$	$0.37 \times (6.50 \times 10^{-11})$	39, 40
$C_2H_5 + H \rightarrow C_2H_6$	1.66×10^{-10}	41
$C_2H_5 \rightarrow C_2H_4 + H$	$6.86 \times 10^{12} \left(\frac{T_g}{298}\right)^{0.95} exp\left(\frac{-1.55 \times 10^5}{RT_g}\right)$	36
$CH_3 + C_2H_3 \rightarrow C_3H_5 + H$	$2.59 \times 10^{-9} \left(\frac{T_g}{298}\right)^{-1.25} exp\left(\frac{-3.21 \times 10^4}{RT_g}\right)$	42

$CH_3 + C_2H_3 \rightarrow C_3H_6$	1.20×10^{-10}	39
$C_2H_3 + H \rightarrow C_2H_4$	2.01×10^{-10}	43
$C_2H_3 \rightarrow C_2H_2 + H$	$2.0 \times 10^{14} exp\left(\frac{-1.66 \times 10^5}{RT_g}\right)$	44
$C_2H_3 + H \rightarrow C_2H_2 + H_2$	3.32×10^{-11}	45
$C_2H_3 + OH \rightarrow CH_3CHO$	5.00×10^{-11}	32
$C_2H_3 + OH \rightarrow CH_3CO + H$	$2.92 \times 10^{-11} \left(\frac{T_g}{298}\right)^{-1.01} exp\left(\frac{-1.621 \times 10^3}{RT_g}\right)$	46
$C_2H_3 + OH \rightarrow CH_3 + CHO$	$2.88 \times 10^{-10} \left(\frac{T_g}{298}\right)^{-1.85} exp\left(\frac{-4.166 \times 10^3}{RT_g}\right)$	46
$C_2H_3 + OH \rightarrow CH_2CO + H_2$	$2.22 \times 10^{-12} \left(\frac{T_g}{298}\right)^{-1.52} exp\left(\frac{-3.018 \times 10^3}{RT_g}\right)$	46
$C_2H_2 + H \rightarrow C_2H_3$	$9.13 \times 10^{-12} exp\left(\frac{-1.01 \times 10^4}{RT_g}\right)$	45
$C_2H_2 \rightarrow C_2H + H$	$2.63 \times 10^{15} exp\left(\frac{-5.19 \times 10^5}{RT_g}\right)$	32
$2CH_3 \rightarrow C_2H_6$	$4.08 \times 10^{-11} \left(\frac{T_g}{298}\right)^{-0.40}$	45
$CH_3 + H \rightarrow CH_4$	3.50×10^{-10}	38
$CH_3 + CH_3CO \rightarrow C_2H_6 + CO$	$0.38 \times (1.43 \times 10^{-10})$	47
$CH_3 \rightarrow CH_2 + H$	$1.90 \times 10^{16} \left(\frac{T_g}{298}\right)^{0.09} exp\left(\frac{-4.59 \times 10^5}{RT_g}\right)$	48
$CH_4 \rightarrow CH_3 + H$	$3.72 \times 10^{15} exp\left(\frac{-4.34 \times 10^5}{RT_g}\right)$	32
$C_2H_6 \rightarrow 2CH_3$	$1.54 \times 10^{18} \left(\frac{T_g}{298}\right)^{-1.24} exp\left(\frac{-3.80 \times 10^5}{RT_g}\right)$	38
$CH + CH \rightarrow C_2H_2$	1.99×10^{-10}	49
$CH + H_2 \rightarrow CH_3$	$2.01 \times 10^{-10} \left(\frac{T_g}{298}\right)^{0.15}$	50
$C_3H_8 \rightarrow C_2H_5 + CH_3$	$2.78 \times 10^{18} \left(\frac{T_g}{298}\right)^{-1.80} exp\left(\frac{-3.71 \times 10^5}{RT_g}\right)$	51
$C_3H_7 + H \rightarrow C_3H_8$	6.00×10^{-11}	52
$C_3H_6 + H \rightarrow C_3H_7$	$6.64 \times 10^{-12} exp\left(\frac{-1.10 \times 10^4}{RT_g}\right)$	45
$C_3H_5 + H \rightarrow C_3H_6$	$2.64 \times 10^{-10} \left(\frac{T_g}{298}\right)^{0.18} exp\left(\frac{5.24 \times 10^2}{RT_g}\right)$	53
$CH + C_2H_5 \rightarrow C_3H_5 + H$	$3.8 \times 10^{-8} T_g^{-0.859} exp\left(\frac{-33.5}{T_g}\right)$	54
$2C_2H_5 \rightarrow C_4H_{10}$	1.66×10^{-11}	45
$C_4H_{10} \rightarrow C_3H_7 + CH_3$	$2.00 \times 10^{16} exp\left(\frac{-3.40 \times 10^5}{RT_g}\right)$	45
$C_4H_{10} \rightarrow C_2H_5 + C_2H_5$	$2.00 \times 10^{16} exp\left(\frac{-3.40 \times 10^5}{RT_g}\right)$	45

$C_2H_6 + C_4H_9 \rightarrow C_4H_{10} + C_2H_5$	$8.30 \times 10^{-13} exp\left(\frac{-6.28 \times 10^4}{RT_g}\right)$	55
$C_4H_{10} + O \rightarrow C_4H_9 + OH$	$7.06 \times 10^{-12} \left(\frac{T_g}{298}\right)^{2.40} exp\left(\frac{-2.30 \times 10^4}{RT_g}\right)$	56
$C_4H_{10} + OH \rightarrow C_4H_9 + H_2O$	$1.31 \times 10^{-12} \left(\frac{T_g}{298}\right)^{1.73} exp\left(\frac{-3.151 \times 10^3}{RT_g}\right)$	57
$C_4H_{10} \rightarrow C_4H_9 + H$	$1.58 \times 10^{16} exp\left(\frac{-4.10 \times 10^5}{RT_g}\right)$	37
$C_4H_{10} + HO_2 \rightarrow C_4H_9 + H_2O_2$	$1.86 \times 10^{-11} exp\left(\frac{-8.11 \times 10^4}{RT_g}\right)$	58
$C_4H_{10} + H \rightarrow C_4H_9 + H_2$	$3.05 \times 10^{-12} \left(\frac{T_g}{298}\right)^{2.54} exp\left(\frac{-2.92 \times 10^4}{RT_g}\right)$	59
$C_4H_{10} + CH_3 \rightarrow C_4H_9 + CH_4$	$3.01 \times 10^{-15} \left(\frac{T_g}{298}\right)^{3.65} exp\left(\frac{-3.03 \times 10^4}{RT_g}\right)$	59
$C_4H_9 \rightarrow C_4H_8 + H$	$1.10 \times 10^{13} \left(\frac{T_g}{298}\right)^{0.25} exp\left(\frac{-1.49 \times 10^5}{RT_g}\right)$	36
$C_4H_9 \rightarrow C_2H_4 + C_2H_5$	$3.70 \times 10^{13} exp\left(\frac{-1.20 \times 10^5}{RT_g}\right)$	45
$C_4H_9 \rightarrow C_3H_6 + CH_3$	$1.26 \times 10^{12} exp\left(\frac{-1.13 \times 10^5}{RT_g}\right)$	60
$C_4H_9 + O_2 \rightarrow C_4H_8 + HO_2$	4.48×10^{-13}	61
$C_2H_4 + C_2H_5 \rightarrow C_4H_8 + H$	8.63×10^{-17}	62
$C_2H_3 + C_2H_5 \rightarrow C_4H_8$	6.50×10^{-11}	39
$C_3H_5 + CH_3 \rightarrow C_4H_8$	$2.72 \times 10^{-11} \left(\frac{T_g}{298}\right)^{-0.32} exp\left(\frac{5.49 \times 10^2}{RT_g}\right)$	63
$2C_4H_9 \rightarrow C_4H_{10} + C_4H_8$	$6.61 \times 10^{-10} exp\left(\frac{-5.438 \times 10^3}{RT_g}\right)$	60
$CH_3 + C_4H_9 \rightarrow CH_4 + C_4H_8$	2.46×10^{-11}	64
$2C_2H_4 \rightarrow C_4H_8$	$6.96 \times 10^{-14} exp\left(\frac{-1.50 \times 10^5}{RT_g}\right)$	65
$C_3H_6 + CH_2 \rightarrow C_4H_8$	$1.35 \times 10^{-11} \left(\frac{T_g}{298}\right)^{-0.15} exp\left(\frac{-1.18 \times 10^1}{RT_g}\right)$	66
$C_4H_8 + H \rightarrow C_4H_9$	$7.59 \times 10^{-12} \left(\frac{T_g}{298}\right)^{0.51} exp\left(\frac{-1.10 \times 10^4}{RT_g}\right)$	36
$C_4H_8 + H \rightarrow C_2H_4 + C_2H_5$	$5.71 \times 10^{-11} exp\left(\frac{-1.64 \times 10^4}{RT_g}\right)$	67
$C_4H_8 + H \rightarrow C_3H_6 + CH_3$	$6.53 \times 10^{-11} exp\left(\frac{-9.578 \times 10^3}{RT_g}\right)$	67
$CHO + H \rightarrow CH_2O$	$7.77 \times 10^{-14} exp\left(\frac{1.90 \times 10^4}{RT_g}\right)$	68
$CH_2OH \rightarrow CH_2O + H$	$1.16 \times 10^{17} \left(\frac{T_g}{298}\right)^{-7.11} exp\left(\frac{-1.84 \times 10^5}{RT_g}\right)$	69
$CH_3O \rightarrow CH_2O + H$	$1.69 \times 10^{14} \left(\frac{T_g}{298}\right)^{-0.39} exp\left(\frac{-1.10 \times 10^5}{RT_g}\right)$	36

$CH_3 + OH \rightarrow CH_3OH$	1.00×10^{-10}	38
$CH_3 + CO \rightarrow CH_3CO$	$8.40 \times 10^{-13} exp\left(\frac{-2.88 \times 10^4}{RT_g}\right)$	38
$CH_2O + O_2 \rightarrow CHO + HO_2$	$3.40 \times 10^{-11} exp\left(\frac{-1.63 \times 10^5}{RT_g}\right)$	32
$H + CH_3CHO \rightarrow CH_3CO + H_2$	$6.64 \times 10^{-11} exp\left(\frac{-1.76 \times 10^4}{RT_g}\right)$	45
$CH_3CO + H \rightarrow CH_3CHO$	$1.50 \times 10^{-10} \left(\frac{T_g}{298}\right)^{0.16}$	46
$C_2H_5 + O_2 \rightarrow CH_3CHO + OH$	$1.0 \times 10^{-13} exp\left(\frac{-2.87 \times 10^4}{RT_g}\right)$	32
$CH_3CHO + H \rightarrow CO + H_2 + CH_3$	$4.88 \times 10^{-13} \left(\frac{T_g}{298}\right)^{2.75} exp\left(\frac{-4.041 \times 10^3}{RT_g}\right)$	70
$CH_3CHO + O_2 \rightarrow CH_3CO + HO_2$	$5.0 \times 10^{-11} exp\left(\frac{-1.64 \times 10^5}{RT_g}\right)$	44
$CH_3CHO + C_2H_3 \rightarrow C_2H_4 + CH_3CO$	$1.35 \times 10^{-13} exp\left(\frac{-1.54 \times 10^4}{RT_g}\right)$	71
$CH + H_2O \rightarrow CH_2OH$	$9.48 \times 10^{-12} exp\left(\frac{3.159 \times 10^3}{RT_g}\right)$	72
$CH_3CO + O_2 \rightarrow CO_2 + CH_3O$	$7.37 \times 10^{-14} exp\left(\frac{4.506 \times 10^3}{RT_g}\right)$	73
$CH_3O + H \rightarrow CH_3OH$	$1.59 \times 10^{-10} \left(\frac{T_g}{298}\right)^{0.24} exp\left(\frac{2.17 \times 10^2}{RT_g}\right)$	74
$CH_3O + HO_2 \rightarrow CH_3OH + O_2$	4.70×10^{-11}	75
$CO + CH_3O \rightarrow CH_2O + CHO$	3.26×10^{-33}	76
$CH_3CHO + H \rightarrow CH_4 + CHO$	8.80×10^{-14}	77
$CHO + H \rightarrow O + CH_2$	$6.61 \times 10^{-11} exp\left(\frac{-4.29 \times 10^5}{RT_g}\right)$	78
$CHO \rightarrow CO + H$	$2.0 \times 10^{5} exp\left(\frac{-1.10 \times 10^5}{RT_g}\right)$	79
$CH_3 + CHO \rightarrow CH_3CHO$	3.01×10^{-11}	32
$CH_3 + O_2 \rightarrow CH_2O + OH$	$2.81 \times 10^{-13} exp\left(\frac{-4.14 \times 10^4}{RT_g}\right)$	80, 81
$CH_3 + OH \rightarrow CH_2O + H_2$	$2.59 \times 10^{-13} \left(\frac{T_g}{298}\right)^{-0.53} exp\left(\frac{-4.52 \times 10^4}{RT_g}\right)$	82
$CH_3O + CH_3CO \rightarrow CH_2O + CH_3CHO$	1.0×10^{-11}	32
$CH_3O_2 + HO_2 \rightarrow CH_2O + H_2O + O_2$	$1.60 \times 10^{-15} exp\left(\frac{-1.44 \times 10^4}{RT_g}\right)$	83
$CH_3O_2 + CH_2OH \rightarrow CH_2O + CH_3OOH$	$4.75 \times 10^{-18} \left(\frac{T_g}{298}\right)^{2.69} exp\left(\frac{-1.43 \times 10^4}{RT_g}\right)$	84
$CH_3O_2 \rightarrow CH_2O + OH$	$5.86 \times 10^{10} \left(\frac{T_g}{298}\right)^{2.98} exp\left(\frac{-1.63 \times 10^5}{RT_g}\right)$	85

$C_3H_5 + O_2 \rightarrow CH_2O + C_2H_2 + OH$	$3.37 \times 10^{-10} \left(\frac{T_g}{298}\right)^{-2.70} exp\left(\frac{-1.05 \times 10^5}{RT_g}\right)$	86
$CH_3OH + OH \rightarrow CH_2O + H_2O + H$	$1.10 \times 10^{-12} \left(\frac{T_g}{298}\right)^{1.44} exp\left(\frac{-4.74 \times 10^2}{RT_g}\right)$	87
$CH_2O + H \rightarrow CH_2OH$	$2.41 \times 10^{-13} \left(\frac{T_g}{298}\right)^{-1.40} exp\left(\frac{-2.17 \times 10^4}{RT_g}\right)$	69
$CH_2O + H \rightarrow CH_3O$	$3.99 \times 10^{-11} exp\left(\frac{-1.72 \times 10^4}{RT_g}\right)$	36
$HCOOH \rightarrow CO + H_2O$	$9.12 \times 10^{12} exp\left(\frac{-2.52 \times 10^5}{RT_g}\right)$	88
$CH_2OH + HO_2 \rightarrow HCOOH + H_2O$	$1.18 \times 10^{-11} \left(\frac{T_g}{298}\right)^{0.12} exp\left(\frac{-1.9 \times 10^3}{RT_g}\right)$	89
$CH_3CHOH + O \rightarrow HCOOH + CH_3$	$3.90 \times 10^{-10} \left(\frac{T_g}{298}\right)^{0.18} exp\left(\frac{-4.07}{RT_g}\right)$	90
$CH_3O_2 + CH_2OH \rightarrow HCOOH + CH_3OH$	$2.34 \times 10^{-17} \left(\frac{T_g}{298}\right)^{2.74} exp\left(\frac{1.49 \times 10^4}{RT_g}\right)$	84
$CO + H_2O \rightarrow HCOOH$	$5.11 \times 10^{-15} \left(\frac{T_g}{298}\right)^{3.10} exp\left(\frac{-2.43 \times 10^5}{RT_g}\right)$	91
$CH_2O + OH \rightarrow HCOOH + H$	2.01×10^{-13}	92
$HCOOH \rightarrow CO_2 + H_2$	$4.46 \times 10^{13} exp\left(\frac{-2.86 \times 10^5}{RT_g}\right)$	93
$HCOOH + OH \rightarrow H_2O + HCOO$	$2.26 \times 10^{-14} exp\left(\frac{-6.535 \times 10^3}{RT_g}\right)$	94
$HCOOH + OH \rightarrow COOH + H_2O$	$9.85 \times 10^{-13} exp\left(\frac{-8.614 \times 10^3}{RT_g}\right)$	94
$CO + H_2O_2 \rightarrow COOH + OH$	$9.60 \times 10^{-14} \left(\frac{T_g}{298}\right)^{2.09} exp\left(\frac{-2.28 \times 10^4}{RT_g}\right)$	95
$CO + OH \rightarrow COOH$	$9.34 \times 10^{-13} \left(\frac{T_g}{298}\right)^{-3.5} exp\left(\frac{-5.478 \times 10^3}{RT_g}\right)$	96
$COOH + O_2 \rightarrow CO_2 + HO_2$	2.09×10^{-12}	97
$COOH \rightarrow CO + OH$	$29.85 \left(\frac{T_g}{298}\right)^{0.13} exp\left(\frac{-1.53 \times 10^5}{RT_g}\right)$	98
$COOH \rightarrow CO_2 + H$	$1.25 \times 10^{2} \left(\frac{T_g}{298}\right)^{0.41} exp\left(\frac{-1.48 \times 10^5}{RT_g}\right)$	98
$COOH + O \rightarrow CO_2 + OH$	1.44×10^{-11}	99
$COOH + OH \rightarrow CO_2 + H_2O$	1.03×10^{-11}	100
$HCOO \rightarrow CO + OH$	$1.21 \times 10^{14} \left(\frac{T_g}{298}\right)^{0.53} exp\left(\frac{-1.42 \times 10^5}{RT_g}\right)$	101
$HCOO \rightarrow CO_2 + H$	$1.0 \times 10^{13} \left(\frac{T_g}{298}\right)^{0.31} exp\left(\frac{-1.38 \times 10^5}{RT_g}\right)$	101
$CH_3O_2 + CH_2OH \rightarrow CH_3O + HOCH_2O$	$1.67 \times 10^{-13} \left(\frac{T_g}{298}\right)^{0.89} exp\left(\frac{1.04 \times 10^4}{RT_g}\right)$	84
$CH_2O + OH \rightarrow HOCH_2O$	$1.13 \times 10^{-13} \left(\frac{T_g}{298}\right)^{1.63} exp\left(\frac{-1.79 \times 10^4}{RT_g}\right)$	102

$HOCH_2O \rightarrow HCOOH + H$	$1.0 \times 10^{14} exp\left(\frac{-6.24 \times 10^4}{RT_g}\right)$	103
$O_2 + HOCH_2O \rightarrow HCOOH + HO_2$	3.50×10^{-14}	104
$CH_2CO + CH_2 \rightarrow C_2H_4 + CO$	2.09×10^{-10}	105
$CH_2CO + H \rightarrow CH_3CO$	$2.66 \times 10^{-11} exp\left(\frac{-6.279 \times 10^3}{RT_g}\right)$	106
$CH_2CO + OH \rightarrow CH_2O + CHO$	4.65×10^{-11}	107
$CH_2CO + CH_3 \rightarrow CO + C_2H_5$	$9.54 \times 10^{-14} \left(\frac{T_g}{298}\right)^{2.29} exp\left(\frac{-4.45 \times 10^4}{RT_g}\right)$	108
$CH_2CO + CH_2 \rightarrow CH_3 + C_2HO$	1.0×10^{-17}	109
$CH_2CO + O \rightarrow C_2HO + OH$	$3.11 \times 10^{-10} exp\left(\frac{-6.98 \times 10^4}{RT_g}\right)$	110
$CH_2CO + CH_3 \rightarrow CH_4 + C_2HO$	$5.94 \times 10^{-14} \left(\frac{T_g}{298}\right)^{3.38} exp\left(\frac{-4.40 \times 10^4}{RT_g}\right)$	108
$2CH_3CO \rightarrow CH_3CHO + CH_2CO$	1.49×10^{-11}	111
$CH_3 + CH_3CO \rightarrow CH_4 + CH_2CO$	1.01×10^{-11}	111
$CH_3CHO \rightarrow CH_2CO + H_2$	$3.0 \times 10^{14} exp\left(\frac{-3.51 \times 10^5}{RT_g}\right)$	112
$CH_3CO \rightarrow CH_2CO + H$	$6.54 \times 10^{-4} \left(\frac{T_g}{298}\right)^{-4.34} exp\left(\frac{-1.94 \times 10^5}{RT_g}\right)$	113
$OH + C_2HO \rightarrow CH_2CO + O$	$1.76 \times 10^{-13} \left(\frac{T_g}{298}\right)^{1.99} exp\left(\frac{-4.72 \times 10^4}{RT_g}\right)$	110
$C_2H_5O + H \rightarrow C_2H_5OH$	$8.32 \times 10^{-11} \left(\frac{T_g}{298}\right)^{0.89} exp\left(\frac{-54.04}{RT_g}\right)$	114
$CH_3 + CH_2OH \rightarrow C_2H_5OH$	2.01×10^{-11}	115
$C_2H_5 + OH \rightarrow C_2H_5OH$	1.28×10^{-10}	116
$C_2H_5O + C_2H_6 \rightarrow C_2H_5OH + C_2H_5$	$4.0 \times 10^{-13} exp\left(\frac{-2.968 \times 10^4}{RT_g}\right)$ Rate Coefficient taken from: $CH_3O + C_2H_6 \rightarrow CH_3OH + C_2H_5$	32
$C_2H_5O + CHO \rightarrow C_2H_5OH + CO$	1.50×10^{-10} Rate Coefficient taken from: $CH_3O + CHO \rightarrow CH_3OH + CO$	32
$C_2H_5O \rightarrow CH_2O + CH_3$	$1.0 \times 10^{15} exp\left(\frac{-9.06 \times 10^4}{RT_g}\right)$	117
$C_2H_5OH + H \rightarrow C_2H_5 + H_2O$	$9.80 \times 10^{-13} exp\left(\frac{-1.45 \times 10^4}{RT_g}\right)$	118
$C_2H_5OH + OH \rightarrow C_2H_5O + H_2O$	$1.67 \times 10^{-14} \left(\frac{T_g}{298}\right)^{3.15} exp\left(\frac{2.380 \times 10^3}{RT_g}\right)$	119
$C_2H_5OH \rightarrow C_2H_4 + H_2O$	$6.91 \times 10^{16} \left(\frac{T_g}{298}\right)^{-3.68} exp\left(\frac{-2.96 \times 10^5}{RT_g}\right)$	120

$C_2H_5OH \rightarrow CH_3 + CH_2OH$	$7.91 \times 10^{24} \left(\frac{T_g}{298}\right)^{-10.59} exp\left(\frac{-4.22 \times 10^5}{RT_g}\right)$	120
$C_2H_5OH \rightarrow C_2H_5 + OH$	$1.34 \times 10^{17} \left(\frac{T_g}{298}\right)^{-2.16} exp\left(\frac{-4.04 \times 10^5}{RT_g}\right)$	121
$C_2H_5OH \rightarrow C_2H_5O + H$	$1.53 \times 10^{16} \left(\frac{T_g}{298}\right)^{0.31} exp\left(\frac{-4.24 \times 10^5}{RT_g}\right)$	114
$C_2H_5OH \rightarrow CH_3CHOH + H$	$1.57 \times 10^{16} \left(\frac{T_g}{298}\right)^{-0.28} exp\left(\frac{-3.93 \times 10^5}{RT_g}\right)$	114
$C_2H_5OH + H \rightarrow CH_3CHOH + H_2$	$1.64 \times 10^{-11} \left(\frac{T_g}{298}\right)^{-0.33} exp\left(\frac{-2.25 \times 10^4}{RT_g}\right)$	119
$C_2H_5OH + OH \rightarrow CH_3CHOH + H_2O$	$1.38 \times 10^{-12} \left(\frac{T_g}{298}\right)^{1.13} exp\left(\frac{1.903 \times 10^3}{RT_g}\right)$	119
$C_2H_5OH + HO_2 \rightarrow CH_3CHOH + H_2O_2$	$3.09 \times 10^{-10} \left(\frac{T_g}{298}\right)^{-1.81} exp\left(\frac{-6.89 \times 10^4}{RT_g}\right)$	119
$C_2H_5OH + CH_3 \rightarrow CH_4 + CH_3CHOH$	$8.87 \times 10^{-15} \left(\frac{T_g}{298}\right)^{3.37} exp\left(\frac{-3.29 \times 10^4}{RT_g}\right)$	119
$C_2H_5OH + O \rightarrow CH_3CHOH + OH$	1.03×10^{-13}	122
$C_2H_5O \rightarrow CH_3CHO + H$	$1.07 \times 10^{14} \left(\frac{T_g}{298}\right)^{-0.69} exp\left(\frac{-9.30 \times 10^4}{RT_g}\right)$	36
$C_2H_5O + C_2H_5O_2 \rightarrow CH_3CHO + C_2H_5OOH$	1.54×10^{-11}	123
$C_2H_5O + H \rightarrow CH_3 + CH_2OH$	$1.23 \times 10^{-10} \left(\frac{T_g}{298}\right)^{0.70} exp\left(\frac{-1.447 \times 10^3}{RT_g}\right)$	114
$C_2H_5O + H \rightarrow C_2H_5 + OH$	$1.25 \times 10^{-12} \left(\frac{T_g}{298}\right)^{1.27} exp\left(\frac{-1.305 \times 10^3}{RT_g}\right)$	114
$C_2H_5O + H \rightarrow CH_3CHO + H_2$	$8.69 \times 10^{-12} \left(\frac{T_g}{298}\right)^{1.15} exp\left(\frac{-2.819 \times 10^3}{RT_g}\right)$	114
$C_2H_5O + H \rightarrow C_2H_4 + H_2O$	$9.69 \times 10^{-12} \left(\frac{T_g}{298}\right)^{-0.81} exp\left(\frac{-2.985 \times 10^3}{RT_g}\right)$	114
$C_2H_5O + H \rightarrow CH_2O + CH_4$	$3.88 \times 10^{-16} \left(\frac{T_g}{298}\right)^{2.21} exp\left(\frac{7.52 \times 10^2}{RT_g}\right)$	114
$CH_3CHO + H \rightarrow C_2H_5O$	$1.33 \times 10^{-11} exp\left(\frac{-2.68 \times 10^4}{RT_g}\right)$	36
$CH_2O + CH_3 \rightarrow C_2H_5O$	$4.98 \times 10^{-13} exp\left(\frac{-2.65 \times 10^4}{RT_g}\right)$	36
$C_2H_5 + O_2 \rightarrow C_2H_5O + O$	$6.14 \times 10^{-12} \left(\frac{T_g}{298}\right)^{-0.20} exp\left(\frac{-1.17 \times 10^5}{RT_g}\right)$	124
$C_2H_5 + HO_2 \rightarrow C_2H_5O + OH$	4.98×10^{-11}	124
$C_2H_5O_2 + O_3 \rightarrow C_2H_5O + 2O_2$	9.27×10^{-18}	125
$2C_2H_5O_2 \rightarrow CH_3CHO + C_2H_5O + HO_2$	$1.21 \times 10^{-15} exp\left(\frac{-0.07}{RT_g}\right)$	126
$C_2H_5O_2 \rightarrow C_2H_5O + O$	$1.78 \times 10^{15} \left(\frac{T_g}{298}\right)^{-0.09} exp\left(\frac{-2.58 \times 10^5}{RT_g}\right)$	127

$C_2H_5 + O \rightarrow C_2H_5O$	$6.31 \times 10^{-11} \left(\frac{T_g}{298}\right)^{0.03} exp\left(\frac{1.648 \times 10^{3}}{RT_g}\right)$	128
$C_2H_5 + O_3 \rightarrow C_2H_5O + O_2$	3.32×10^{-14}	129
$C_2H_5OOH \rightarrow C_2H_5O + OH$	$4.0 \times 10^{15} exp\left(\frac{-1.80 \times 10^{5}}{RT_g}\right)$	38
$CH_3CHOH + O_2 \rightarrow CH_3CHO + HO_2$	1.90×10^{-11}	130
$CH_3CHOH + O \rightarrow CH_3CHO + OH$	3.16×10^{-10}	131
$CH_3CHOH + H \rightarrow CH_3CHO + H_2$	3.32×10^{-11}	131
$CH_3CHOH + H \rightarrow CH_3 + CH_2OH$	$8.99 \times 10^{-10} \left(\frac{T_g}{298}\right)^{-0.89} exp\left(\frac{-1.21 \times 10^{4}}{RT_g}\right)$	114
$CH_3CHOH + H \rightarrow C_2H_5O + H$	$9.31 \times 10^{-16} \left(\frac{T_g}{298}\right)^{2.94} exp\left(\frac{-3.55 \times 10^{4}}{RT_g}\right)$	114
$CH_3CHOH + H \rightarrow C_2H_5 + OH$	$3.55 \times 10^{-11} \left(\frac{T_g}{298}\right)^{-0.83} exp\left(\frac{-2.01 \times 10^{4}}{RT_g}\right)$	114
$CH_3CHOH + H \rightarrow C_2H_4 + H_2O$	$2.63 \times 10^{-10} \left(\frac{T_g}{298}\right)^{-3.02} exp\left(\frac{-1.19 \times 10^{4}}{RT_g}\right)$	114
$CH_3CHOH + H \rightarrow CH_2O + CH_4$	$8.73 \times 10^{-17} \left(\frac{T_g}{298}\right)^{2.10} exp\left(\frac{-8.90 \times 10^{2}}{RT_g}\right)$	114
$CH_3CHOH + H \rightarrow C_2H_5OH$	$8.43 \times 10^{-11} \left(\frac{T_g}{298}\right)^{0.06} exp\left(\frac{-1.829 \times 10^{3}}{RT_g}\right)$	114
$CH_3CHOH \rightarrow CH_3CHO + H$	$1.20 \times 10^{15} \left(\frac{T_g}{298}\right)^{-5.19} exp\left(\frac{-1.49 \times 10^{5}}{RT_g}\right)$	132
$CH_3CHOH \rightarrow CH_2O + CH_3$	$1.49 \times 10^{13} \left(\frac{T_g}{298}\right)^{-3.59} exp\left(\frac{-1.45 \times 10^{5}}{RT_g}\right)$	132
$C_2H_5O \rightarrow CH_3CHOH$	$1.87 \left(\frac{T_g}{298}\right)^{12.40} exp\left(\frac{-1.77 \times 10^{4}}{RT_g}\right)$	133
$CH_3CHO + H \rightarrow CH_3CHOH$	$8.02 \times 10^{-13} \left(\frac{T_g}{298}\right)^{2.20} exp\left(\frac{-3.14 \times 10^{4}}{RT_g}\right)$	70
$CH_3CHO + HO_2 \rightarrow CH_3CHOH + O_2$	$4.19 \times 10^{-10} \left(\frac{T_g}{298}\right)^{-1.80} exp\left(\frac{-1.09 \times 10^{5}}{RT_g}\right)$	134
$C_3H_7O \rightarrow C_2H_5CHO + H$	$6.38 \times 10^{12} \left(\frac{T_g}{298}\right)^{0.75} exp\left(\frac{-8.81 \times 10^{4}}{RT_g}\right)$	36
$C_3H_7O \rightarrow CH_2O + C_2H_5$	$2.36 \times 10^{15} \left(\frac{T_g}{298}\right)^{-2.45} exp\left(\frac{-7.10 \times 10^{4}}{RT_g}\right)$	36
$C_3H_7O + O_2 \rightarrow C_2H_5CHO + HO_2$	$1.40 \times 10^{-14} exp\left(\frac{-9.15 \times 10^{2}}{RT_g}\right)$	135
$C_3H_7 + HO_2 \rightarrow OH + C_3H_7O$	4.00×10^{-11}	51
$C_2H_5CHO + H \rightarrow C_3H_7O$	$6.64 \times 10^{-12} exp\left(\frac{-2.62 \times 10^{4}}{RT_g}\right)$	36
$CH_2O + C_2H_5 \rightarrow C_3H_7O$	$1.66 \times 10^{-13} exp\left(\frac{-1.46 \times 10^{4}}{RT_g}\right)$	36
$C_3H_7 + OH \rightarrow C_3H_7OH$	4.00×10^{-11}	51
$CH_2OH + C_2H_5 \rightarrow C_3H_7OH$	2.01×10^{-11}	115

$C_3H_7OH + OH \rightarrow H_2O + C_3H_7O$	$3.23 \times 10^{-14} exp\left(\frac{4.008 \times 10^3}{RT_g}\right)$	136
$C_3H_7OH \rightarrow C_2H_5 + CH_2OH$	$2.70 \times 10^{16} exp\left(\frac{-3.47 \times 10^5}{RT_g}\right)$	137
$C_3H_7OH \rightarrow C_3H_6 + H_2O$	$3.95 \times 10^{13} \left(\frac{T_g}{298}\right)^{0.50} exp\left(\frac{-2.51 \times 10^5}{RT_g}\right)$	138
$C_3H_7 + O_2 \rightarrow C_3H_7O_2$	$1.15 \times 10^{-12} \left(\frac{T_g}{298}\right)^{0.50} exp\left(\frac{4.656 \times 10^3}{RT_g}\right)$	139
$C_3H_6 + HO_2 \rightarrow C_3H_7O_2$	$9.62 \times 10^{-17} \left(\frac{T_g}{298}\right)^{3.27} exp\left(\frac{-4.10 \times 10^4}{RT_g}\right)$	140
$C_3H_7O_2 \rightarrow C_3H_7 + O_2$	$7.46 \times 10^{21} \left(\frac{T_g}{298}\right)^{-12.51} exp\left(\frac{-1.77 \times 10^5}{RT_g}\right)$	141
$C_3H_7O_2 \rightarrow C_2H_5CHO + OH$	$1.74 \times 10^{11} \left(\frac{T_g}{298}\right)^{2.31} exp\left(\frac{1.54 \times 10^5}{RT_g}\right)$	85
$C_3H_7O_2 \rightarrow C_3H_6 + HO_2$	$6.06 \times 10^{20} \left(\frac{T_g}{298}\right)^{-13.03} exp\left(\frac{-1.76 \times 10^5}{RT_g}\right)$	141
$C_2H_5CO \rightarrow C_2H_5 + CO$	$2.09 \times 10^{13} exp\left(\frac{-6.15 \times 10^4}{RT_g}\right)$	142
$CH_2CO \rightarrow CO + CH_2$	$3.00 \times 10^{14} exp\left(\frac{-2.97 \times 10^5}{RT_g}\right)$	45
$C_2H_5 + O_2 \rightarrow C_2H_5O_2$	$1.09 \times 10^{-7} \left(\frac{T_g}{298}\right)^{-10.30} exp\left(\frac{-2.54 \times 10^4}{RT_g}\right)$	124
$C_2H_5O_2 \rightarrow C_2H_5 + O_2$	$5.30 \times 10^{15} \left(\frac{T_g}{298}\right)^{-0.83} exp\left(\frac{-1.43 \times 10^5}{RT_g}\right)$	143
$C_2H_5O_2 \rightarrow CH_3CHO + OH$	$7.27 \times 10^{10} \left(\frac{T_g}{298}\right)^{2.63} exp\left(\frac{-1.55 \times 10^5}{RT_g}\right)$	85
$C_3H_7 + O_2 \rightarrow C_2H_5CHO + OH$	1.83×10^{-16}	144
$C_2H_5 + CHO \rightarrow C_2H_5CHO$	3.01×10^{-11}	32
$CO + C_2H_5 \rightarrow C_2H_5CO$	$2.51 \times 10^{-13} exp\left(\frac{-2.01 \times 10^4}{RT_g}\right)$	32
$C_2H_5CHO + O \rightarrow OH + C_2H_5CO$	$9.43 \times 10^{-12} exp\left(\frac{6.452 \times 10^3}{RT_g}\right)$	145
$C_2H_5CHO + O_2 \rightarrow HO_2 + C_2H_5CO$	5.65×10^{-23}	146
$C_2H_5CHO + OH \rightarrow H_2O + C_2H_5CO$	1.85×10^{-11}	147
$C_2H_5CHO + HO_2 \rightarrow H_2O_2 + C_2H_5CO$	2.52×10^{-15}	148
$C_2H_5CHO + C_2H_5 \rightarrow C_2H_6 + C_2H_5CO$	$8.32 \times 10^{-14} exp\left(\frac{-2.63 \times 10^4}{RT_g}\right)$	80, 149

Ion-ion reactions

Reaction	**Rate coefficient**	**Ref.**
$H^- + CHO^+ \rightarrow 2H + CO$	$3.76 \times 10^{-8} \left(\frac{T_g}{300}\right)^{-0.50}$	150
$H^- + CHO^+ \rightarrow H + CHO$	$3.76 \times 10^{-8} \left(\frac{T_g}{300}\right)^{-0.50}$	150

$O^- + CHO^+ \rightarrow O + H + CO$	$3.76 \times 10^{-8} \left(\frac{T_g}{300}\right)^{-0.50}$	150
$O^- + CHO^+ \rightarrow O + CHO$	$3.76 \times 10^{-8} \left(\frac{T_g}{300}\right)^{-0.50}$	150
$O_2^- + CHO^+ \rightarrow O_2 + H + CO$	$3.76 \times 10^{-8} \left(\frac{T_g}{300}\right)^{-0.50}$	150
$O_2^- + CHO^+ \rightarrow O_2 + CHO$	$3.76 \times 10^{-8} \left(\frac{T_g}{300}\right)^{-0.50}$	150
$OH^- + CHO^+ \rightarrow OH + H + CO$	$3.76 \times 10^{-8} \left(\frac{T_g}{300}\right)^{-0.50}$	150
$OH^- + CHO^+ \rightarrow OH + CHO$	$3.76 \times 10^{-8} \left(\frac{T_g}{300}\right)^{-0.50}$	150
$O^- + C^+ \rightarrow C + O$	$7.51 \times 10^{-8} \left(\frac{T_g}{300}\right)^{-0.50}$	150
$O^- + C_2H_2^+ \rightarrow O + C_2H_2$	$7.51 \times 10^{-8} \left(\frac{T_g}{300}\right)^{-0.50}$	150
$O^- + C_2H_3^+ \rightarrow O + C_2H_3$	$7.51 \times 10^{-8} \left(\frac{T_g}{300}\right)^{-0.50}$	150
$O^- + CH_3^+ \rightarrow O + CH_3$	$7.51 \times 10^{-8} \left(\frac{T_g}{300}\right)^{-0.50}$	150
$O_2^- + C^+ \rightarrow C + O_2$	$7.51 \times 10^{-8} \left(\frac{T_g}{300}\right)^{-0.50}$	150
$O_2^- + C_2H_2^+ \rightarrow O_2 + C_2H_2$	$7.51 \times 10^{-8} \left(\frac{T_g}{300}\right)^{-0.50}$	150
$O_2^- + C_2H_3^+ \rightarrow O_2 + C_2H_3$	$7.51 \times 10^{-8} \left(\frac{T_g}{300}\right)^{-0.50}$	150
$O_2^- + CH_3^+ \rightarrow O_2 + CH_3$	$7.51 \times 10^{-8} \left(\frac{T_g}{300}\right)^{-0.50}$	150
$OH^- + C_2H_2^+ \rightarrow OH + C_2H_2$	$7.51 \times 10^{-8} \left(\frac{T_g}{300}\right)^{-0.50}$	150
$OH^- + C_2H_3^+ \rightarrow OH + C_2H_3$	$7.51 \times 10^{-8} \left(\frac{T_g}{300}\right)^{-0.50}$	150
$OH^- + CH_3^+ \rightarrow OH + CH_3$	$7.51 \times 10^{-8} \left(\frac{T_g}{300}\right)^{-0.50}$	150
$H^- + C_2H_2^+ \rightarrow H + C_2H_2$	$7.51 \times 10^{-8} \left(\frac{T_g}{300}\right)^{-0.50}$	150
$H^- + C_2H_3^+ \rightarrow H + C_2H_3$	$7.51 \times 10^{-8} \left(\frac{T_g}{300}\right)^{-0.50}$	150
$H^- + CH_3^+ \rightarrow H + CH_3$	$7.51 \times 10^{-8} \left(\frac{T_g}{300}\right)^{-0.50}$	150
$H^- + H_3O^+ \rightarrow 2H + H_2O$	$7.51 \times 10^{-8} \left(\frac{T_g}{300}\right)^{-0.50}$	150

Ion-neutral reactions

Reaction	**Rate coefficient**	**Ref.**
$O^- + O_2 \rightarrow O_2^- + O$	7.30×10^{-10}	150
$CH_2 + O^- \rightarrow CH_2O + e^-$	5.00×10^{-10}	150

$CH + O^- \rightarrow CHO + e^-$	5.00×10^{-10}	150
$C^+ + C_3H_6 \rightarrow C_2H_2^+ + C_2H_4$	3.00×10^{-10}	150
$C^+ + C_3H_6 \rightarrow C_2H_3^+ + C_2H_3$	6.00×10^{-10}	150
$H_3^+ + C_2H_5OH \rightarrow C_2H_3^+ + H_2O + 2H_2$	$4.00 \times 10^{-10} \left(\frac{T_g}{300}\right)^{-0.50}$	150
$H_3^+ + C_3H_6 \rightarrow C_2H_3^+ + CH_4 + H_2$	9.00×10^{-10}	150
$H_3^+ + CH_3CHO \rightarrow C_2H_3^+ + H_2 + H_2O$	$8.97 \times 10^{-10} \left(\frac{T_g}{300}\right)^{-0.50}$	150
$C^+ + CH_3OH \rightarrow CHO + CH_3^+$	$2.08 \times 10^{-9} \left(\frac{T_g}{300}\right)^{-0.50}$	150
$CH^+ + CH_3OH \rightarrow CH_2O + CH_3^+$	$1.45 \times 10^{-9} \left(\frac{T_g}{300}\right)^{-0.50}$	150
$CH^+ + CH_2O \rightarrow CO + CH_3^+$	$9.60 \times 10^{-10} \left(\frac{T_g}{300}\right)^{-0.50}$	150
$CH_2^+ + CHO \rightarrow CO + CH_3^+$	$4.50 \times 10^{-10} \left(\frac{T_g}{300}\right)^{-0.50}$	150
$H^+ + CH_3OH \rightarrow CH_3^+ + H_2O$	$5.90 \times 10^{-10} \left(\frac{T_g}{300}\right)^{-0.50}$	150
$H_3^+ + C_2H_5OH \rightarrow CH_3^+ + CH_4 + H_2O$	$1.50 \times 10^{-9} \left(\frac{T_g}{300}\right)^{-0.50}$	150
$H_3^+ + CH_3CHO \rightarrow CH_3^+ + CH_3OH$	$1.45 \times 10^{-9} \left(\frac{T_g}{300}\right)^{-0.50}$	150
$H_3^+ + CH_3OH \rightarrow CH_3^+ + H_2O + H_2$	$3.71 \times 10^{-9} \left(\frac{T_g}{300}\right)^{-0.50}$	150
$C^+ + CHO \rightarrow CHO^+ + C$	$4.80 \times 10^{-10} \left(\frac{T_g}{300}\right)^{-0.50}$	150
$C_2^+ + CHO \rightarrow CHO^+ + C_2$	$3.80 \times 10^{-10} \left(\frac{T_g}{300}\right)^{-0.50}$	150
$C_2H_2^+ + CHO \rightarrow CHO^+ + C_2H_2$	$5.00 \times 10^{-10} \left(\frac{T_g}{300}\right)^{-0.50}$	150
$CH^+ + CHO \rightarrow CHO^+ + CH$	$4.60 \times 10^{-10} \left(\frac{T_g}{300}\right)^{-0.50}$	150
$CH_3^+ + CHO \rightarrow CH_3 + CHO^+$	$4.40 \times 10^{-10} \left(\frac{T_g}{300}\right)^{-0.50}$	150
$CO^+ + CHO \rightarrow CO + CHO^+$	$7.40 \times 10^{-10} \left(\frac{T_g}{300}\right)^{-0.50}$	150
$H^+ + CHO \rightarrow CHO^+ + H$	$9.40 \times 10^{-10} \left(\frac{T_g}{300}\right)^{-0.50}$	150
$H_2^+ + CHO \rightarrow CHO^+ + H_2$	$1.00 \times 10^{-9} \left(\frac{T_g}{300}\right)^{-0.50}$	150
$H_2O^+ + CHO \rightarrow CHO^+ + H_2O$	$2.80 \times 10^{-10} \left(\frac{T_g}{300}\right)^{-0.50}$	150
$CHO + O_2^+ \rightarrow CHO^+ + O_2$	$3.60 \times 10^{-10} \left(\frac{T_g}{300}\right)^{-0.50}$	150
$O^+ + CHO \rightarrow CHO^+ + O$	$4.30 \times 10^{-10} \left(\frac{T_g}{300}\right)^{-0.50}$	150

$OH^+ + CHO \rightarrow OH + CHO^+$	$2.80 \times 10^{-10} \left(\frac{T_g}{300}\right)^{-0.50}$	150
$C^+ + CH_2O \rightarrow CHO^+ + CH$	$7.80 \times 10^{-10} \left(\frac{T_g}{300}\right)^{-0.50}$	150
$C^+ + H_2O \rightarrow CHO^+ + H$	$9.00 \times 10^{-10} \left(\frac{T_g}{300}\right)^{-0.50}$	150
$C_2H + CO^+ \rightarrow CHO^+ + C_2$	3.90×10^{-10}	150
$C + H_3O^+ \rightarrow CHO^+ + H_2$	1.00×10^{-11}	150
$CH^+ + CO_2 \rightarrow CHO^+ + CO$	1.60×10^{-9}	150
$CH^+ + CH_2O \rightarrow CHO^+ CH_2$	$9.60 \times 10^{-10} \left(\frac{T_g}{300}\right)^{-0.50}$	150
$CH^+ + H_2O \rightarrow CHO^+ + H_2$	$2.90 \times 10^{-9} \left(\frac{T_g}{300}\right)^{-0.50}$	150
$CH^+ + O_2 \rightarrow CHO^+ + O$	9.70×10^{-10}	150
$CH_2^+ + CH_2O \rightarrow CHO^+ + CH_3$	$2.81 \times 10^{-9} \left(\frac{T_g}{300}\right)^{-0.50}$	150
$CH_2^+ + O_2 \rightarrow CHO^+ + OH$	9.10×10^{-10}	150
$CH_2^+ + O \rightarrow CHO^+ + H$	7.50×10^{-10}	150
$CH_2 + CO^+ \rightarrow CHO^+ + CH$	4.30×10^{-10}	150
$CH_3^+ + CH_2O \rightarrow CHO^+ + CH_4$	$1.60 \times 10^{-9} \left(\frac{T_g}{300}\right)^{-0.50}$	150
$CH_3^+ + O \rightarrow CHO^+ + H_2$	4.00×10^{-10}	150
$CH_4^+ + CO \rightarrow CHO^+ + CH_3$	1.40×10^{-9}	150
$CH_4 + CO^+ \rightarrow CHO^+ + CH_3$	4.55×10^{-10}	150
$CH_5^+ + CO \rightarrow CHO^+ + CH_4$	1.00×10^{-9}	150
$CH + CO^+ \rightarrow CHO^+ + C$	$3.20 \times 10^{-10} \left(\frac{T_g}{300}\right)^{-0.50}$	150
$CH + O_2^+ \rightarrow CHO^+ + O$	$3.10 \times 10^{-10} \left(\frac{T_g}{300}\right)^{-0.50}$	150
$CO^+ + CH_2O \rightarrow CHO^+ + CHO$	$1.65 \times 10^{-9} \left(\frac{T_g}{300}\right)^{-0.50}$	150
$H^+ + CH_3OH \rightarrow CHO^+ + 2H_2$	$8.85 \times 10^{-10} \left(\frac{T_g}{300}\right)^{-0.50}$	150
$H^+ + CO_2 \rightarrow CHO^+ + O$	3.50×10^{-9}	150
$H^+ + CH_2O \rightarrow CHO^+ + H_2$	$3.57 \times 10^{-9} \left(\frac{T_g}{300}\right)^{-0.50}$	150
$H_2^+ + CO \rightarrow CHO^+ + H$	2.16×10^{-9}	150
$H_2^+ + CH_2O \rightarrow CHO^+ + H_2 + H$	$1.40 \times 10^{-9} \left(\frac{T_g}{300}\right)^{-0.50}$	150
$H_2 + CO^+ \rightarrow CHO^+ + H$	7.50×10^{-10}	150
$CH_2O + O_2^+ \rightarrow O_2 + CHO^+ + H$	$2.30 \times 10^{-10} \left(\frac{T_g}{300}\right)^{-0.50}$	150
$H_2O^+ + CO \rightarrow CHO^+ + OH$	5.00×10^{-10}	150

$H_2O + CO^+ \rightarrow CHO^+ + OH$	$8.84 \times 10^{-10} \left(\frac{T_g}{300}\right)^{-0.50}$	150
$H_3^+ + CO \rightarrow CHO^+ + H_2$	$1.36 \times 10^{-9} \left(\frac{T_g}{300}\right)^{-0.14} exp\left(\frac{3.40}{T_g}\right)$	150
$H + CO_2^+ \rightarrow CHO^+ + O$	2.90×10^{-10}	150
$O^+ + CH_2O \rightarrow CHO^+ + OH$	$1.40 \times 10^{-9} \left(\frac{T_g}{300}\right)^{-0.50}$	150
$C_2H_2 + O_2^+ \rightarrow CHO^+ + H + CO$	6.50×10^{-11}	150
$O + C_2H^+ \rightarrow CHO^+ + C$	3.30×10^{-10}	150
$O + C_2H_2^+ \rightarrow CHO^+ + CH$	8.50×10^{-11}	150
$O + C_2H_4^+ \rightarrow CHO^+ + CH_3$	8.40×10^{-11}	150
$OH^+ + CO \rightarrow CHO^+ + O$	1.05×10^{-9}	150
$OH + CO^+ \rightarrow CHO^+ + O$	$3.10 \times 10^{-10} \left(\frac{T_g}{300}\right)^{-0.50}$	150
$C_2 + CHO^+ \rightarrow CO + C_2H^+$	8.30×10^{-10}	150
$C_2H_2 + CHO^+ \rightarrow C_2H_3^+ + CO$	1.40×10^{-9}	150
$C_2H_3 + CHO^+ \rightarrow C_2H_4^+ + CO$	$1.40 \times 10^{-9} \left(\frac{T_g}{300}\right)^{-0.50}$	150
$C_2H_4 + CHO^+ \rightarrow C_2H_5^+ + CO$	1.40×10^{-9}	150
$C_2H + CHO^+ \rightarrow C_2H_2^+ + CO$	7.80×10^{-10}	150
$C + CHO^+ \rightarrow CH^+ + CO$	1.10×10^{-9}	150
$CH_2 + CHO^+ \rightarrow CO + CH_3^+$	8.60×10^{-10}	150
$CH + CHO^+ \rightarrow CO + CH_2^+$	$6.30 \times 10^{-10} \left(\frac{T_g}{300}\right)^{-0.50}$	150
$H_2O + CHO^+ \rightarrow CO + H_3O^+$	$2.50 \times 10^{-9} \left(\frac{T_g}{300}\right)^{-0.50}$	150
$CHO^+ + C_2H_5 \rightarrow C_2H_6^+ + CO$	1.40×10^{-9}	150
$OH + CHO^+ \rightarrow CO + H_2O^+$	$6.20 \times 10^{-10} \left(\frac{T_g}{300}\right)^{-0.50}$	150

Electron-ion dissociative recombination

Reaction	**Rate coefficient**	**Ref.**
$CHO^+ + e^- \rightarrow H + CO$	$0.88 \times 2.4 \times 10^{-7} \left(\frac{T_e}{300}\right)^{-0.69}$	151,152
$CHO^+ + e^- \rightarrow C + OH$	$0.06 \times 2.4 \times 10^{-7} \left(\frac{T_e}{300}\right)^{-0.69}$	151,152
$CHO^+ + e^- \rightarrow CH + O$	$0.06 \times 2.4 \times 10^{-7} \left(\frac{T_e}{300}\right)^{-0.69}$	151,152

Table S7. Calculated values of the minimum power density that is sustained in the afterglows, the maximum power density reached in the pulses, and the effective period by which molecules are exposed to pulses, for different plasma powers.

Plasma Power (W)	**Minimum power density ($W\ cm^{-3}$)**	**Maximum power density ($W\ cm^{-3}$)**	**Effective pulse period (ms)**
8.0	7.97	3.72×10^5	5.55
10.4	10.2	4.74×10^5	4.27
13.8	13.2	6.14×10^5	3.22
17.9	16.6	7.73×10^5	2.48

4. Simulation Results

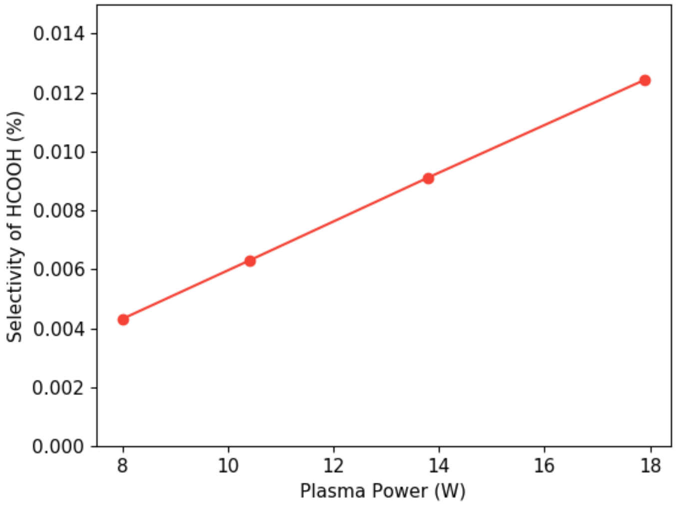

Figure S8. Calculated selectivity of formic acid at different plasma powers.

Species Production and Destruction Reactions in Plasma.

We provide here the main (production and destruction) reactions occurring in the plasma for the most important molecules, as well as some radicals. As a DBD consists of filaments, the chemistry is clearly different in these filaments (called pulses; characterized by higher plasma power) compared to the space in between filaments (called afterglows; characterized by lower plasma power).

4.1. C_2H_6

Destruction

Destruction of C_2H_6 occurs mainly through electron impact dissociation in the pulses:

$$C_2H_6 + e^- \rightarrow C_2H_4 + H_2 + e^- \tag{R1.1}$$

$$C_2H_6 + e^- \rightarrow C_2H_5 + H + e^- \tag{R1.2}$$

$$C_2H_6 + e^- \rightarrow C_2H_2 + 2H_2 + e^- \tag{R1.3}$$

$$C_2H_6 + e^- \rightarrow 2CH_3 + e^- \tag{R1.4}$$

$$C_2H_6 + e^- \rightarrow CH_4 + CH_2 + e^- \tag{R1.5}$$

$$C_2H_6 + e^- \rightarrow C_2H_3 + H_2 + H + e^- \tag{R1.6}$$

With (preset) branching ratios for electron impact dissociation of (0.46, 0.24, 0.11, 0.08, 0.07 and 0.04), respectively.

A smaller, but still relevant amount of C_2H_6 destruction occurs in the afterglows through reactions with radicals:

$$C_2H_6 + OH \rightarrow C_2H_5 + H_2O \tag{R1.7}$$

$$C_2H_6 + O \rightarrow C_2H_5 + OH \tag{R1.8}$$

$$C_2H_6 + H \rightarrow C_2H_5 + H_2 \tag{R1.9}$$

The rates of (R1.1-R1.9) decrease at higher C_2H_6 conversions, as less C_2H_6 is available and as a higher fraction of the OH, O and H radicals will react away with the formed products.

Production

Production of C_2H_6 occurs mainly in the afterglows through recombination and disproportionation reactions with radicals:

$$C_2H_5 + H \rightarrow C_2H_6 \qquad (R1.10)$$

$$2CH_3 \rightarrow C_2H_6 \qquad (R1.11)$$

$$2C_2H_5 \rightarrow C_2H_4 + C_2H_6 \qquad (R1.12)$$

$$C_2H_5 + CHO \rightarrow C_2H_6 + CO \qquad (R1.13)$$

At low conversions, destruction reactions are more important in the afterglows, while at high conversions, the productions reactions become more important in the afterglows.

4.2. CO_2

Destruction

Destruction of CO_2 occurs mainly in the pulses by electron impact dissociation:

$$CO_2 + e^- \rightarrow CO + O + e^- \qquad (R2.1)$$

And to some extent in the afterglows through:

$$CH_2 + CO_2 \rightarrow CH_2O + CO \qquad (R2.2)$$

Under the investigated conditions and at the calculated CO_2 conversions, the formation of CO_2 is not important relative to its destruction.

4.3. CO

Production

The production of CO occurs both in the pulses and in the afterglows. The most important reaction in the pulses is electron impact dissociation of CO_2 (R2.1):

$$CO_2 + e^- \rightarrow CO + O + e^- \qquad (R2.1)$$

The most important reactions for production of CO in the afterglows are:

$$CH_2 + CO_2 \rightarrow CH_2O + CO \qquad (R2.2)$$

$$C_2H_5 + CHO \rightarrow C_2H_6 + CO \qquad (R3.1)$$

$$C_2H_2 + O \rightarrow CH_2 + CO \qquad (R3.2)$$

$$C_2H_5CO \rightarrow C_2H_5 + CO \qquad (R3.3)$$

Destruction

Destruction of CO occurs mainly in the afterglows through reaction:

$$C_2H_5 + CO \rightarrow C_2H_5CO \qquad (R3.4)$$

And to a lesser extent through:

$$CH_3 + CO \rightarrow CH_3CO \qquad (R3.5)$$

However, most of the C_2H_5CO is formed through reaction R3.4 and decomposes back to CO via R3.3. As a result, the net reaction does not contribute as much to the formation of CO, compared to the other formation reactions listed.

4.4. C_2H_4

Production

Formation of C_2H_4 occurs mainly through electron impact dissociation of C_2H_6 in the pulse:

$$C_2H_6 + e^- \rightarrow C_2H_4 + H_2 + e^- \qquad (R1.1)$$

And also to some extent by disproportionation of C_2H_x radicals in the afterglows:

$$C_2H_5 + C_2H_3 \rightarrow C_2H_4 + C_2H_2 \qquad (R4.1)$$

$$C_2H_5 + C_2H_5 \rightarrow C_2H_4 + C_2H_4 \qquad (R4.2)$$

Destruction:

Destruction of C_2H_4 in the pulses happens through electron impact dissociation:

$$C_2H_4 + e^- \rightarrow C_2H_2 + H_2 + e^- \qquad (R4.3)$$

$$C_2H_4 + e^- \rightarrow C_2H_3 + H + e^- \qquad (R4.4)$$

$$C_2H_4 + e^- \rightarrow C_2H_2 + 2H + e^- \qquad (R4.5)$$

And by recombination and oxidation reactions in the afterglows:

$$C_2H_4 + H \rightarrow C_2H_5 \qquad (R4.6)$$

$$C_2H_4 + O \rightarrow CH_3 + CHO \qquad (R4.7)$$

4.5. C_2H_2

Production

C_2H_2 is mainly formed in the pulses through electron impact reaction of C_2H_6 and C_2H_4:

$$C_2H_6 + e^- \rightarrow C_2H_2 + 2H_2 + e^- \qquad (R1.3)$$

$$C_2H_4 + e^- \rightarrow C_2H_2 + H_2 + e^- \qquad (R4.3)$$

And to a lesser extent also through disproportionation and electron-ion recombination reactions in the afterglows:

$$C_2H_5 + C_2H_3 \rightarrow C_2H_4 + C_2H_2 \qquad (R4.1)$$

$$CH_3 + C_2H_3 \rightarrow CH_4 + C_2H_2 \qquad (R5.1)$$

$$e^- + C_2H_4^+ \rightarrow C_2H_2 + 2H \qquad (R5.2)$$

Destruction

Destruction of C_2H_2 occurs in the afterglows through oxidation and recombination:

$$C_2H_2 + O \rightarrow CH_2 + CO \tag{R3.2}$$

$$C_2H_2 + H \rightarrow C_2H_3 \tag{R5.3}$$

4.6. CH_4

Production

Production of CH_4 occurs through electron impact dissociation of higher hydrocarbons in the pulses:

$$C_2H_6 + e^- \rightarrow CH_4 + CH_2 + e^- \tag{R1.5}$$

$$C_3H_8 + e^- \rightarrow C_2H_4 + CH_4 + e^- \tag{R6.1}$$

$$C_3H_6 + e^- \rightarrow C_2H_2 + CH_4 + e^- \tag{R6.2}$$

As well as through recombination and disproportionation reactions between radicals in the afterglows:

$$CH_3 + H \rightarrow CH_4 \tag{R6.3}$$

$$CH_3 + CHO \rightarrow CH_4 + CO \tag{R6.4}$$

Destruction

Destruction of CH_4 occurs mainly through electron impact reactions in the pulses:

$$CH_4 + e^- \rightarrow CH_3 + H + e^- \tag{R6.5}$$

$$CH_4 + e^- \rightarrow CH_2 + H_2 + e^- \tag{R6.6}$$

4.7. C_3H_8

Production

C_3H_8 is produced through recombination of radicals in the afterglows:

$$CH_3 + C_2H_5 \rightarrow C_3H_8 \qquad (R7.1)$$

Destruction

Destruction happens through electron impact reactions in the pulses:

$$C_3H_8 + e^- \rightarrow C_3H_6 + H_2 + e^- \qquad (R7.2)$$

$$C_3H_8 + e^- \rightarrow C_2H_4 + CH_4 + e^- \qquad (R7.3)$$

$$C_3H_8 + e^- \rightarrow C_3H_7 + H + e^- \qquad (R7.4)$$

4.8. C_4H_{10}

Production

C_4H_{10} is formed through recombination in the afterglows:

$$C_2H_5 + C_2H_5 \rightarrow C_4H_{10} \qquad (R8.1)$$

Destruction

Electron impact reactions of C_4 hydrocarbons are not included in the model (no cross sections are available), and as a result there are no important destruction reactions for this product.

4.9. C_3H_6

Production

The formation of C_3H_6 occurs through electron impact dissociation of C_3H_8 in the pulses, and reactions between radicals in the afterglows:

$$C_3H_8 + e^- \rightarrow C_3H_6 + H_2 + e^- \qquad (R7.2)$$

$$CH_3 + C_2H_3 \rightarrow C_3H_6 \qquad (R9.1)$$

$$C_4H_8 + H \rightarrow C_3H_6 + CH_3 \quad (R9.2)$$

Destruction

Destruction occurs by electron impact dissociation in the pulses and recombination with CH_2 radicals in the afterglows:

$$C_3H_6 + e^- \rightarrow C_2H_2 + CH_4 + e^- \quad (R9.3)$$

$$C_3H_6 + e^- \rightarrow C_3H_5 + H + e^- \quad (R9.4)$$

$$C_3H_6 + CH_2 \rightarrow C_4H_8 \quad (R9.5)$$

4.10. C_4H_8

Production

Production of C_4H_8 occurs through recombination reactions in the afterglows:

$$C_3H_6 + CH_2 \rightarrow C_4H_8 \quad (R9.5)$$

$$C_2H_5 + C_2H_3 \rightarrow C_4H_8 \quad (R10.1)$$

Where R9.5 becomes more important at higher conversions.

Destruction

Destruction of C_4H_8 occurs in the afterglows (as no electron impact reactions could be included for C_4 hydrocarbons) through:

$$C_4H_8 + H \rightarrow C_3H_6 + CH_3 \quad (R10.2)$$

$$C_4H_8 + H \rightarrow C_2H_4 + C_2H_5 \quad (R10.3)$$

4.11. CH_2O

Production

Formation of CH_2O happens in the afterglows through:

$$CH_2 + CO_2 \rightarrow CH_2O + CO \quad (R2.2)$$

$$C_2H_5 + O \rightarrow CH_3 + CH_2O \quad (R11.1)$$

$$C_2H_5O \rightarrow CH_3 + CH_2O \qquad (R11.2)$$

$$C_3H_7O \rightarrow C_2H_5 + CH_2O \qquad (R11.3)$$

R11.1 and R11.2 are more important at low conversion, while R11.3 becomes more important at higher conversions. However, R11.3 is largely counteracted by its reverse reaction (R11.5, see below) so that the net rate is not important.

Destruction

The destruction of CH_2O occurs in the afterglows by the following reactions:

$$CH_2O + H \rightarrow CH_3O \qquad (R11.4)$$

$$CH_2O + C_2H_5 \rightarrow C_3H_7O \qquad (R11.5)$$

$$CH_2O + H \rightarrow CHO + H_2 \qquad (R11.6)$$

$$CH_2O + O \rightarrow CHO + OH \qquad (R11.7)$$

$$CH_2O + OH \rightarrow CHO + H_2O \qquad (R11.8)$$

Note that reactions R11.3 and R11.5 largely cancel each other out especially at higher conversions.

4.12. CH_3CHO

Production

Production of CH_3CHO (acetaldehyde) occurs in the afterglows through oxidation of C_2H_5 radicals or by recombination between CH_3 and CHO radicals:

$$C_2H_5 + O \rightarrow CH_3CHO + H \qquad (R12.1)$$

$$CH_3 + CHO \rightarrow CH_3CHO \qquad (R12.2)$$

Destruction

Destruction also occurs in the afterglows through reaction with H, O and OH radicals:

$$H + CH_3CHO \rightarrow H_2 + CH_3CO \qquad (R12.3)$$

$$H + CH_3CHO \rightarrow H_2 + CH_3 + CO \qquad (R12.4)$$

$$O + CH_3CHO \rightarrow OH + CH_3CO \qquad (R12.5)$$

$$OH + CH_3CHO \rightarrow H_2O + CH_3CO \qquad (R12.6)$$

CH_3CO primarily decomposes into CO and CH_3:

$$CH_3CO \rightarrow CH_3 + CO \qquad (R12.7)$$

4.13. C_2H_5CHO

C_2H_5CHO (propanal) is formed in the afterglows via recombination:

$$C_2H_5 + CHO \rightarrow C_2H_5CHO \qquad (R13.1)$$

Destruction also happens in the afterglows by:

$$C_2H_5CHO + O \rightarrow C_2H_5CO + OH \qquad (R13.2)$$

$$C_2H_5CHO + OH \rightarrow C_2H_5CO + H_2O \qquad (R13.3)$$

4.14. CH_3OH

Production

Production of CH_3OH happens in the afterglows by:

$$CH_3 + OH \rightarrow CH_3OH \qquad (R14.1)$$

$$CH_3O + H \rightarrow CH_3OH \qquad (R14.2)$$

$$CH_3O + C_2H_6 \rightarrow CH_3OH + C_2H_5 \qquad (R14.3)$$

$$CH_3O + CHO \rightarrow CH_3OH + CO \qquad (R14.4)$$

$$CH_3O + CH_2O \rightarrow CH_3OH + CHO \qquad (R14.5)$$

The importance of R14.1 relative to the total production decreases at higher conversions, while that of R14.4 and R14.5 increases with conversion.

Destruction

Destruction of CH_3OH occurs in the afterglows by:

$$CH_3OH + O \rightarrow OH + CH_2OH \qquad (R14.6)$$

$$CH_3OH + O \rightarrow OH + CH_3O \qquad (R14.7)$$

$$CH_3OH + OH \rightarrow H_2O + CH_3O \qquad (R14.8)$$

$$CH_3OH + OH \rightarrow CH_2O + H_2O + H \qquad (R14.9)$$

$$H + CH_3OH \rightarrow CH_2OH + H_2 \qquad (R14.10)$$

Most CH_3O reacts to form CH_2O, CH_2OH reacts to form alcohols or formaldehyde:

$$CH_3O + CH_3 \rightarrow CH_2O + CH_4 \qquad (R14.11)$$

$$CH_3O + C_2H_5 \rightarrow CH_2O + C_2H_6 \qquad (R14.12)$$

$$CH_2OH + C_2H_5 \rightarrow C_3H_7OH \qquad (R14.13)$$

$$CH_2OH + CH_3 \rightarrow C_2H_5OH \qquad (R14.14)$$

$$CH_2OH + CHO \rightarrow CH_3OH + CO \qquad (R14.15)$$

$$CH_2OH + CHO \rightarrow 2CH_2O \qquad (R14.16)$$

4.15. C_2H_5OH

Production

Production happens in the afterglows through:

$$C_2H_5 + OH \rightarrow C_2H_5OH \qquad (R15.1)$$

$$C_2H_5O + H \rightarrow C_2H_5OH \qquad (R15.2)$$

$$C_2H_5O + CHO \rightarrow C_2H_5OH + CO \qquad (R15.3)$$

$$C_2H_5O + C_2H_6 \rightarrow C_2H_5OH + C_2H_5 \qquad (R15.4)$$

the C_2H_5O radical is formed by recombination of C_2H_5 and O:

$$C_2H_5 + O \rightarrow C_2H_5O \tag{R15.5}$$

Destruction

Destruction of C_2H_5OH occurs in the afterglows by:

$$C_2H_5OH + H \rightarrow C_2H_5 + H_2O \tag{R15.6}$$

$$C_2H_5OH + H \rightarrow CH_3CHOH + H_2 \tag{R15.7}$$

$$C_2H_5OH + O \rightarrow CH_3CHOH + OH \tag{R15.8}$$

$$C_2H_5OH + OH \rightarrow CH_3CHOH + H_2O \tag{R15.9}$$

4.16. HCOOH

Production

HCOOH (formic acid) is formed through oxidation reactions in the afterglows:

$$CH_2O + OH \rightarrow HCOOH + H \tag{R16.1}$$

$$CH_3CHOH + O \rightarrow HCOOH + CH_3 \tag{R16.2}$$

Destruction

The rate of destruction is much less important compared to that of production under the conditions investigated and at the conversion reached during the residence time.

4.17. CHO radicals

Production

The CHO radical is formed in the afterglows by:

$$C_2H_4 + O \rightarrow CH_3 + CHO \tag{R4.7}$$

$$CH_2O + O \rightarrow CHO + OH \tag{R11.7}$$

Destruction

Destruction mainly happens through:

$$C_2H_5 + CHO \rightarrow C_2H_6 + CO \tag{R1.13}$$

$$CH_3 + CHO \rightarrow CH_4 + CO \tag{R6.4}$$

4.18. CH_3CHOH radicals

Production

This radical is mainly formed from C_2H_5OH in the afterglows:

$$C_2H_5OH + H \rightarrow CH_3CHOH + H_2 \tag{R15.7}$$

$$C_2H_5OH + O \rightarrow CH_3CHOH + OH \tag{R15.8}$$

$$C_2H_5OH + OH \rightarrow CH_3CHOH + H_2O \tag{R15.9}$$

Destruction

The radical is oxidized in the afterglows to form HCOOH and CH_3CHO:

$$CH_3CHOH + O \rightarrow HCOOH + CH_3 \tag{R16.2}$$

$$CH_3CHOH + O \rightarrow CH_3CHO + OH \tag{R18.1}$$

References

(1) Winter, Lea R.; Ashford, Bryony; Hong, Jungmi; Murphy, Anthony B.; Chen, Jingguang G. Identifying Surface Reaction Intermediates in Plasma Catalytic Ammonia Synthesis. *ACS Catal.* **2020**, *10* (24), 14763–14774. https://doi.org/10.1021/acscatal.0c03166.

(2) Kriegseis, Jochen; Möller, Benjamin; Grundmann, Sven; Tropea, Cameron. Capacitance and Power Consumption Quantification of Dielectric Barrier Discharge (DBD) Plasma Actuators. *J. Electrostat.* **2011**, *69* (4), 302–312. https://doi.org/10.1016/j.elstat.2011.04.007.

(3) Liu, Shuang; Winter, Lea R.; Chen, Jingguang G. Review of Plasma-Assisted Catalysis for Selective Generation of Oxygenates from CO_2 and CH_4. *ACS Catal.* **2020**, *10* (4), 2855–2871. https://doi.org/10.1021/acscatal.9b04811.

(4) Ramakers, Marleen; Michielsen, Inne; Aerts, Robby; Meynen, Vera; Bogaerts, Annemie. Effect of Argon or Helium on the CO_2 Conversion in a Dielectric Barrier Discharge. *Plasma Process. Polym.* **2015**, *12* (8), 755–763. https://doi.org/10.1002/ppap.201400213.

(5) Xie, Zhenhua; Xu, Yuanguo; Xie, Meng; Chen, Xiaobo; Lee, Ji Hoon; Stavitski, Eli; Kattel, Shyam; Chen, Jingguang G. Reactions of CO_2 and Ethane Enable CO Bond Insertion for Production of C_3 Oxygenates. *Nat. Commun.* **2020**, *11* (1), 1–8.

(6) Kim, Jongsik; Go, David B.; Hicks, Jason C. Synergistic Effects of Plasma-Catalyst Interactions for CH_4 Activation. *Phys. Chem. Chem. Phys.* **2017**, *19* (20), 13010–13021. https://doi.org/10.1039/c7cp01322a.

(7) Winter, Lea R.; Chen, Rui; Chen, Xin; Chang, Kuan; Liu, Zongyuan; Senanayake, Sanjaya D.; Ebrahim, Amani M.; Chen, Jingguang G. Elucidating the Roles of Metallic Ni and Oxygen Vacancies in CO_2 Hydrogenation over Ni/CeO_2 Using Isotope Exchange and in Situ Measurements. *Appl. Catal. B Environ.* **2019**, *245*, 360–366. https://doi.org/10.1016/j.apcatb.2018.12.069.

(8) Zhang, Xiuling; Zhu, Aimin; Li, Xuehui; Gong, Weimin. Oxidative Dehydrogenation of Ethane with CO_2 over Catalyst under Pulse Corona Plasma. *Catal. Today* **2004**, *89* (1–2), 97–102. https://doi.org/10.1016/j.cattod.2003.11.015.

(9) Gómez-Ramírez, Ana; Rico, Victor J.; Cotrino, José; González-Elipe, Agustín R.; Lambert, Richard M. Low Temperature Production of Formaldehyde from Carbon Dioxide and Ethane by Plasma-Assisted Catalysis in a Ferroelectrically Moderated Dielectric Barrier Discharge Reactor. *ACS Catal.* **2014**, *4* (2), 402–408. https://doi.org/10.1021/cs4008528.

(10) Neyts, Erik C.; Ostrikov, Kostya; Sunkara, Mahendra K.; Bogaerts, Annemie. Plasma Catalysis: Synergistic Effects at the Nanoscale. *Chem. Rev.* **2015**, *115* (24), 13408–13446. https://doi.org/10.1021/acs.chemrev.5b00362.

(11) Pancheshnyi, S.; Eismann, B.; Hagelaar, G. J. M.; Pitchford, L. C. Computer Code ZDPlasKin. (University of Toulouse, LAPLACE, CNRS-UPS-INP, Toulouse, France). 2008.

(12) Hagelaar, G. J. M.; Pitchford, L. C. Solving the Boltzmann Equation to Obtain Electron Transport Coefficients and Rate Coefficients for Fluid Models. *Plasma Sources Sci. Technol.* **2005**, *14* (4), 722–733. https://doi.org/10.1088/0963-0252/14/4/011.

(13) van 't Veer, K.; Engelmann, Y.; Reniers, F.; Bogaerts, A. Plasma-Catalytic Ammonia Synthesis in a DBD Plasma: Role of Microdischarges and Their Afterglows. *J. Phys. Chem. C* **2020**, *124* (42), 22871–22883. https://doi.org/10.1021/acs.jpcc.0c05110.

(14) van 't Veer, K.; Reniers, F.; Bogaerts, A. Zero-Dimensional Modeling of Unpacked and Packed Bed Dielectric Barrier Discharges: The Role of Vibrational Kinetics in Ammonia Synthesis. *Plasma Sources Sci. Technol.* **2020**, *29* (4), 045020. https://doi.org/10.1088/1361-6595/ab7a8a.

(15) Vermeiren, Vincent; Bogaerts, Annemie. Plasma-Based CO_2 Conversion: To Quench or Not to Quench? *J. Phys. Chem. C* **2020**, *124* (34), 18401–18415. https://doi.org/10.1021/acs.jpcc.0c04257.

(16) Cleiren, Emelie; Heijkers, Stijn; Ramakers, Marleen; Bogaerts, Annemie. Dry Reforming of Methane in a Gliding Arc Plasmatron: Towards a Better Understanding of the Plasma Chemistry. *ChemSusChem* **2017**, *10* (20), 4025–4036. https://doi.org/10.1002/cssc.201701274.

(17) Slaets, Joachim; Aghaei, Maryam; Ceulemans, Sara; Van Alphen, Senne; Bogaerts, Annemie. CO_2 and CH_4 Conversion in "Real" Gas Mixtures in a Gliding Arc Plasmatron: How Do N_2 and O_2 Affect the Performance? *Green Chem.* **2020**, *22* (4), 1366–1377. https://doi.org/10.1039/C9GC03743H.

(18) Heijkers, Stijn; Aghaei, Maryam; Bogaerts, Annemie. Plasma-Based CH_4 Conversion into Higher Hydrocarbons and H_2: Modeling to Reveal the Reaction Mechanisms of Different Plasma Sources. *J. Phys. Chem. C* **2020**, *124* (13), 7016–7030. https://doi.org/10.1021/acs.jpcc.0c00082.

(19) Morillo-Candas, A. S.; Silva, T.; Klarenaar, B. L. M.; Grofulović, M.; Guerra, V.; Guaitella, O. Electron

Impact Dissociation of CO_2. *Plasma Sources Sci. Technol.* **2020**, *29* (1), 01LT01. https://doi.org/10.1088/1361-6595/ab6075.

(20) Polak, L. S.; Slovetsky, D. I. Electron Impact Induced Electronic Excitation and Molecular Dissociation. *Int. J. Radiat. Phys. Chem.* **1976**, *8* (1–2), 257–282. https://doi.org/10.1016/0020-7055(76)90070-X.

(21) Hake, R. D.; Phelps, A. V. Momentum-Transfer and Inelastic-Collision Cross Sections for Electrons in O_2, CO, and CO_2. *Phys. Rev.* **1967**, *158* (1), 70–84. https://doi.org/10.1103/PhysRev.158.70.

(22) Janev, R. K.; Reiter, D. Collision Processes of $C_{2,3}H_y$ and $C_{2,3}H_y^+$ Hydrocarbons with Electrons and Protons. *Phys. Plasmas* **2004**, *11* (2), 780–829. https://doi.org/10.1063/1.1630794.

(23) Hayashi Database, www.lxcat.net, Retrieved on May 7, 2021.

(24) Morgan Database, www.lxcat.net, Retrieved on May 7, 2021.

(25) Puech Database, www.lxcat.net, Retrieved on May 7, 2021.

(26) Ozkan, A.; Dufour, T.; Silva, T.; Britun, N.; Snyders, R.; Bogaerts, A.; Reniers, F. The Influence of Power and Frequency on the Filamentary Behavior of a Flowing DBD—Application to the Splitting of CO_2. *Plasma Sources Sci. Technol.* **2016**, *25* (2), 025013. https://doi.org/10.1088/0963-0252/25/2/025013.

(27) Bogaerts, Annemie; Wang, Weizong; Berthelot, Antonin; Guerra, Vasco. Modeling Plasma-Based CO_2 Conversion: Crucial Role of the Dissociation Cross Section. *Plasma Sources Sci. Technol.* **2016**, *25* (5), 055016. https://doi.org/10.1088/0963-0252/25/5/055016.

(28) Hayashi, Makoto. Electron Collision Cross-Sections for Molecules Determined from Beam and Swarm Data. In *Swarm Studies and Inelastic Electron-Molecule Collisions*; Springer New York: New York, NY, 1987; pp 167–187. https://doi.org/10.1007/978-1-4612-4662-6_33.

(29) Hayashi, Makoto. Electron Collision Cross-Sections Determined from Beam and Swarm Data by Boltzmann Analysis; 1990; Vol. 220, pp 333–340. https://doi.org/10.1007/978-1-4615-3780-9_21.

(30) Fresnet, F.; Pasquiers, S.; Postel, C.; Puech, V. Dynamics and Breakdown Delay Times in Neon-Ethene and Neon-Propene Photo-Triggered Discharges. *J. Phys. D. Appl. Phys.* **2002**, *35* (9), 308. https://doi.org/10.1088/0022-3727/35/9/308.

(31) Mahmud, Khaled; Marshall, Paul; Fontijn, Arthur. A High-Temperature Photochemistry Kinetics Study of the Reaction of Oxygen(3P) Atoms with Ethylene from 290 to 1510 K. *J. Phys. Chem.* **1987**, *91* (6), 1568–1573. https://doi.org/10.1021/j100290a056.

(32) Tsang, W.; Hampson, R. F. Chemical Kinetic Data Base for Combustion Chemistry. Part I. Methane and Related Compounds. *J. Phys. Chem. Ref. Data* **1986**, *15* (3), 1087–1279. https://doi.org/10.1063/1.555759.

(33) Li, Xiaohu; Jasper, Ahren W.; Zádor, Judit; Miller, James A.; Klippenstein, Stephen J. Theoretical Kinetics of O + C_2H_4. *Proc. Combust. Inst.* **2017**, *36* (1), 219–227. https://doi.org/10.1016/j.proci.2016.06.053.

(34) Pruss, Frank J.; Slagle, Irene R.; Gutman, David. Determination of Branching Ratios for the Reaction of Oxygen Atoms with Ethylene. *J. Phys. Chem.* **1974**, *78* (7), 663–665. https://doi.org/10.1021/j100600a003.

(35) Vasu, Subith S.; Hong, Zekai; Davidson, David F.; Hanson, Ronald K.; Golden, David M. Shock Tube/Laser Absorption Measurements of the Reaction Rates of OH with Ethylene and Propene. *J. Phys. Chem. A* **2010**, *114* (43), 11529–11537. https://doi.org/10.1021/jp106049s.

(36) Curran, H. J. Rate Constant Estimation for C_1 to C_4 Alkyl and Alkoxyl Radical Decomposition. *Int. J. Chem. Kinet.* **2006**, *38* (4), 250–275. https://doi.org/10.1002/kin.20153.

(37) Dean, A. M. Predictions of Pressure and Temperature Effects upon Radical Addition and Recombination Reactions. *J. Phys. Chem.* **1985**, *89* (21), 4600–4608. https://doi.org/10.1021/j100267a038.

(38) Baulch, D. L.; Cobos, C. J.; Cox, R. A.; Frank, P.; Hayman, G.; Just, Th.; Kerr, J. A.; Murrells, T.; Pilling, M. J.; Troe, J.; Walker, R. W.; Warnatz, J. Evaluated Kinetic Data for Combustion Modeling. Supplement I. *J. Phys. Chem. Ref. Data* **1994**, *23* (6), 847–848. https://doi.org/10.1063/1.555953.

(39) Laufer, Allan H.; Fahr, Askar. Reactions and Kinetics of Unsaturated C_2 Hydrocarbon Radicals. *Chem. Rev.* **2004**, *104* (6), 2813–2832. https://doi.org/10.1021/cr030039x.

(40) Ibuki, T.; Takezaki, Y. The Reaction of Hydrogen Atoms with Acetylene. *Bull. Chem. Soc. Jpn.* **1975**, *48* (3), 769–773.

(41) Sillesen, Alfred; Ratajczak, Emil; Pagsberg, Palle. Kinetics of the Reactions $H + C_2H_4 \rightarrow C_2H_5$, $H + C_2H_5 \rightarrow 2CH_3$ and $CH_3 + C_2H_5 \rightarrow$ Products Studied by Pulse Radiolysis Combined with Infrared Diode Las. *Chem. Phys. Lett.* **1993**, *201* (1–4), 171–177. https://doi.org/10.1016/0009-2614(93)85052-P.

(42) Blanquart, G.; Pepiot-Desjardins, P.; Pitsch, H. Chemical Mechanism for High Temperature Combustion of Engine Relevant Fuels with Emphasis on Soot Precursors. *Combust. Flame* **2009**, *156* (3), 588–607. https://doi.org/10.1016/j.combustflame.2008.12.007.

(43) Fahr, A.; Laufer, A.; Klein, R.; Braun, W. Reaction Rate Determinations of Vinyl Radical Reactions with Vinyl, Methyl, and Hydrogen Atoms. *J. Phys. Chem.* **1991**, *95* (8), 3218–3224.

https://doi.org/10.1021/j100161a047.

(44) Baulch, D. L.; Cobos, C. J.; Cox, R. A.; Esser, C.; Frank, P.; Just, Th.; Kerr, J. A.; Pilling, M. J.; Troe, J.; Walker, R. W.; Warnatz, J. Evaluated Kinetic Data for Combustion Modelling. *J. Phys. Chem. Ref. Data* **1992**, *21* (3), 411–734. https://doi.org/10.1063/1.555908.

(45) Warnatz, Jürgen. Rate Coefficients in the C/H/O System. In *Combustion Chemistry*; Springer New York: New York, NY, 1984; pp 197–360. https://doi.org/10.1007/978-1-4684-0186-8_5.

(46) Knyazev, Vadim D. Kinetics and Mechanism of the Reaction of Recombination of Vinyl and Hydroxyl Radicals. *Chem. Phys. Lett.* **2017**, *685*, 165–170. https://doi.org/10.1016/j.cplett.2017.07.040.

(47) Adachi, Hiroyuki; Basco, N.; James, D. G. L. The Acetyl Radicals $CH_3CO\cdot$ and $CD_3CO\cdot$ Studied by Flash Photolysis and Kinetic Spectroscopy. *Int. J. Chem. Kinet.* **1981**, *13* (12), 1251–1276. https://doi.org/10.1002/kin.550131206.

(48) Su, J. Z.; Teitelbaum, H. The Rate of Methyl Radical Decomposition at High Temperatures and Pressures. *Int. J. Chem. Kinet.* **1994**, *26* (1), 159–169. https://doi.org/10.1002/kin.550260116.

(49) Braun, W.; McNesby, J. R.; Bass, Arnold M. Flash Photolysis of Methane in the Vacuum Ultraviolet. II. Absolute Rate Constants for Reactions of CH with Methane, Hydrogen, and Nitrogen. *J. Chem. Phys.* **1967**, *46* (6), 2071–2080. https://doi.org/10.1063/1.1841003.

(50) Fulle, D.; Hippler, H. The Temperature and Pressure Dependence of the Reaction $CH+H_2 \Leftrightarrow CH_3 \Leftrightarrow CH_2+H$. *J. Chem. Phys.* **1997**, *106* (21), 8691–8698. https://doi.org/10.1063/1.473930.

(51) Tsang, Wing. Chemical Kinetic Data Base for Combustion Chemistry. Part 3: Propane. *J. Phys. Chem. Ref. Data* **1988**, *17* (2), 887–951. https://doi.org/10.1063/1.555806.

(52) Gregory P. Smith; Golden, David M.; Frenklach, Michael; Moriarty, Nigel W.; Eiteneer, Boris; Goldenberg, Mikhail; Bowman, C. Thomas; Hanson, Ronald K.; Song, Soonho; Gardiner, William C.; Lissianski, Jr. Vitali V.; Qin, Zhiwei. GRI-MECH 3.0.

(53) Harding, Lawrence B.; Klippenstein, Stephen J.; Georgievskii, Yuri. On the Combination Reactions of Hydrogen Atoms with Resonance-Stabilized Hydrocarbon Radicals. *J. Phys. Chem. A* **2007**, *111* (19), 3789–3801. https://doi.org/10.1021/jp0682309.

(54) Canosa, A.; Sims, I. R.; Travers, D.; Smith, I. W. M.; Rowe, B. R. Reactions of the Methylidine Radical with CH_4, C_2H_2, C_2H_4, C_2H_6, and but-1-Ene Studied between 23 and 295 K with a CRESU Apparatus. *Astron. Astrophys* **1997**, *323* (2), 644–651.

(55) Lin, M. C.; Back, M. H. THE THERMAL DECOMPOSITION OF ETHANE: PART III. SECONDARY REACTIONS. *Can. J. Chem.* **1966**, *44* (20), 2369–2380. https://doi.org/10.1139/v66-358.

(56) Cohen, N.; Westberg, K. R. The Use of Transition-State Theory to Extrapolate Rate Coefficients for Reactions of O Atoms with Alkanes. *Int. J. Chem. Kinet.* **1986**, *18* (1), 99–140. https://doi.org/10.1002/kin.550180109.

(57) Droege, August T.; Tully, Frank P. Hydrogen Atom Abstraction from Alkanes by Hydroxyl. 5. n-Butane. *J. Phys. Chem.* **1986**, *90* (22), 5937–5941. https://doi.org/10.1021/j100280a096.

(58) Pitz, William J.; Westbrook, Charles K. Chemical Kinetics of the High Pressure Oxidation of N-Butane and Its Relation to Engine Knock. *Combust. Flame* **1986**, *63* (1–2), 113–133. https://doi.org/10.1016/0010-2180(86)90115-X.

(59) Manion, Jeffrey A.; Sheen, David A.; Awan, Iftikhar A. Evaluated Kinetics of the Reactions of H and CH_3 with n-Alkanes: Experiments with n-Butane and a Combustion Model Reaction Network Analysis. *J. Phys. Chem. A* **2015**, *119* (28), 7637–7658. https://doi.org/10.1021/acs.jpca.5b01004.

(60) Kerr, J. A.; Trotman-Dickenson, A. F. 323. The Reactions of Alkyl Radicals. Part III. n-Butyl Radicals from the Photolysis of n-Valeraldehyde. *J. Chem. Soc.* **1960**, 1602–1608. https://doi.org/10.1039/jr9600001602.

(61) Baker, Richard R.; Baldwin, Roy R.; Fuller, Alan R.; Walker, Raymond W. Addition of $N\text{-}C_4H_{10}$ and C_4H_8 to Slowly Reacting Mixtures of Hydrogen and Oxygen at 480°C. Part 1.—Formation of Hydrocarbon Products. *J. Chem. Soc. Faraday Trans. 1 Phys. Chem. Condens. Phases* **1975**, *71*, 736–755. https://doi.org/10.1039/f19757100736.

(62) MacKenzie, Allan L.; Pacey, Philip D.; Wimalasena, Jayantha H. Radical Addition, Decomposition, and Isomerization Reactions in the Pyrolysis of Ethane and Ethylene. *Can. J. Chem.* **1984**, *62* (7), 1325–1328. https://doi.org/10.1139/v84-222.

(63) Tsang, Wing. Chemical Kinetic Data Base for Combustion Chemistry Part V. Propene. *J. Phys. Chem. Ref. Data* **1991**, *20* (2), 221–273. https://doi.org/10.1063/1.555880.

(64) Thynne, J. C. J. Reactions of Alkyl Radicals. Part 1.—Methyl Radical Photosensitized Decomposition of Ethyl Formate. *Trans. Faraday Soc.* **1962**, *58* (4), 676–684. https://doi.org/10.1039/TF9625800676.

(65) Silcocks, C. G.; A, Proc R. Soc Lond. The Kinetics of the Thermal Decomposition and Polymerization of

Ethane and Ethylene. *Proc. R. Soc. London. Ser. A. Math. Phys. Sci.* **1956**, *233* (1195), 465–479. https://doi.org/10.1098/rspa.1956.0004.

(66) Polino, Daniela; Klippenstein, Stephen J.; Harding, Lawrence B.; Georgievskii, Yuri. Predictive Theory for the Addition and Insertion Kinetics of $^1CH_2$ Reacting with Unsaturated Hydrocarbons. *J. Phys. Chem. A* **2013**, *117* (48), 12677–12692. https://doi.org/10.1021/jp406246y.

(67) Manion, Jeffrey A.; Awan, Iftikhar A. Evaluated Kinetics of Terminal and Non-Terminal Addition of Hydrogen Atoms to 1-Alkenes: A Shock Tube Study of H + 1-Butene. *J. Phys. Chem. A* **2015**, *119* (3), 429–441. https://doi.org/10.1021/jp5110856.

(68) Tsuboi, Takao; Katoh, Masataka; Kikuchi, Shigeru; Hashimoto, Kazunobu. Thermal Decomposition of Methanol behind Shock Waves. *Jpn. J. Appl. Phys.* **1981**, *20* (5), 985–992.

(69) Xu, Z. F.; Raghunath, P.; Lin, M. C. Ab Initio Chemical Kinetics for the CH_3 + O(3P) Reaction and Related Isomerization–Decomposition of CH_3O and CH_2OH Radicals. *J. Phys. Chem. A* **2015**, *119* (28), 7404–7417. https://doi.org/10.1021/acs.jpca.5b00553.

(70) Sivaramakrishnan, R.; Michael, J. V.; Klippenstein, S. J. Direct Observation of Roaming Radicals in the Thermal Decomposition of Acetaldehyde. *J. Phys. Chem. A* **2010**, *114* (2), 755–764. https://doi.org/10.1021/jp906918z.

(71) Scherzer, Klaus; Löser, Uwe; Stiller, Wolfgang. BSBL-Rechnungen Zu Wasserstoffabspaltungsreaktionen (Durch Alkenylradikale; Vinylradikale. *Zeitschrift für Chemie* **1987**, *27* (8), 300–301. https://doi.org/10.1002/zfch.19870270815.

(72) Zabarnick, S.; Fleming, J. W.; Lin, M. C. Temperature Dependence of CH Radical Reactions with H_2O and CH_2O. *Symp. Combust.* **1988**, *21* (1), 713–719. https://doi.org/10.1016/S0082-0784(88)80303-5.

(73) Hoare, D. E.; Whytock, D. A. Photooxidation of Acetone Vapor. *Can. J. Chem.* **1967**, *45* (8), 865–872. https://doi.org/10.1139/v67-144.

(74) Jasper, Ahren W.; Klippenstein, Stephen J.; Harding, Lawrence B.; Ruscic, Branko. Kinetics of the Reaction of Methyl Radical with Hydroxyl Radical and Methanol Decomposition. *J. Phys. Chem. A* **2007**, *111* (19), 3932–3950. https://doi.org/10.1021/jp067585p.

(75) Assaf, Emmanuel; Schoemaecker, Coralie; Vereecken, Luc; Fittschen, Christa. The Reaction of Fluorine Atoms with Methanol: Yield of CH_3O/CH_2OH and Rate Constant of the Reactions CH_3O + CH_3O and CH_3O + HO_2. *Phys. Chem. Chem. Phys.* **2018**, *20* (16), 10660–10670. https://doi.org/10.1039/c7cp05770a.

(76) Wang, Baoshan; Hou, Hua; Gu, Yueshu. Ab Initio/Density Functional Theory and Multichannel RRKM Calculations for the CH_3O + CO Reaction. *J. Phys. Chem. A* **1999**, *103* (40), 8021–8029. https://doi.org/10.1021/jp991203g.

(77) Lambert, R. M.; Christie, M. I.; Linnett, J. W. A Novel Reaction of Hydrogen Atoms. *Chem. Commun.* **1967**, No. 8, 388–389. https://doi.org/10.1039/c19670000388.

(78) Tsuboi, Takao; Hashimoto, Kazunobu. Shock Tube Study on Homogeneous Thermal Oxidation of Methanol. *Combust. Flame* **1981**, *42* (C), 61–76. https://doi.org/10.1016/0010-2180(81)90142-5.

(79) Trenwith, A. B. 847. The Thermal Decomposition of Acetaldehyde: The Formation of Hydrogen. *J. Chem. Soc.* **1963**, 4426–4430. https://doi.org/10.1039/jr9630004426.

(80) Manion, J. A. et al. NIST Chemical Kinetics Database, NIST Standard Reference Database 17, Version 7.0 (Web Version), Release 1.6.8, Data version 2015.09, National Institute of Standards and Technology, Gaithersburg, Maryland, 20899-8320.

(81) Teitel'boim, M. A.; Romanovich, L. B.; Vedeneev, B. I. Calculation, Based on RRKM Theory, of Certain Channels of Interaction of Methyl Radical with Oxygen. *Kinet. Catal.* **1973**, *19*, 1131–1136.

(82) Dean, A. M.; Westmoreland, P. R. Bimolecular QRRK Analysis of Methyl Radical Reactions. *Int. J. Chem. Kinet.* **1987**, *19* (3), 207–228. https://doi.org/10.1002/kin.550190305.

(83) Elrod, Matthew J.; Ranschaert, Dana L.; Schneider, Nicholas J. Direct Kinetics Study of the Temperature Dependence of the CH2O Branching Channel for the CH_3O_2 + HO_2 Reaction. *Int. J. Chem. Kinet.* **2001**, *33* (6), 363–376. https://doi.org/10.1002/kin.1030.

(84) Zhao, Zhongrui; Song, Jinou; Su, Boyang; Wang, Xiaowen; Li, Zhijun. Mechanistic Study of the Reactions of Methyl Peroxy Radical with Methanol or Hydroxyl Methyl Radical. *J. Phys. Chem. A* **2018**, *122* (23), 5078–5088. https://doi.org/10.1021/acs.jpca.7b09988.

(85) Villano, Stephanie M.; Huynh, Lam K.; Carstensen, Hans-Heinrich; Dean, Anthony M. High-Pressure Rate Rules for Alkyl + O_2 Reactions. 1. The Dissociation, Concerted Elimination, and Isomerization Channels of the Alkyl Peroxy Radical. *J. Phys. Chem. A* **2011**, *115* (46), 13425–13442. https://doi.org/10.1021/jp2079204.

(86) Lee, Jongwoo; Bozzelli, Joseph W. Thermochemical and Kinetic Analysis of the Allyl Radical with O_2

Reaction System. *Proc. Combust. Inst.* **2005**, *30* (1), 1015–1022. https://doi.org/10.1016/j.proci.2004.08.092.

(87) Srinivasan, N. K.; Su, M. C.; Michael, J. V. High-Temperature Rate Constants for CH_3OH + Kr → Products, OH + CH_3OH → Products, OH + $(CH_3)_2CO$ → CH_2COCH_3 + H_2O, and OH + CH_3 → CH_2 + H_2O. *J. Phys. Chem. A* **2007**, *111* (19), 3951–3958. https://doi.org/10.1021/jp0673516.

(88) Elwardany, A.; Nasir, E. F.; Es-sebbar, Et.; Farooq, A. Unimolecular Decomposition of Formic and Acetic Acids: A Shock Tube/Laser Absorption Study. *Proc. Combust. Inst.* **2015**, *35* (1), 429–436. https://doi.org/10.1016/j.proci.2014.06.141.

(89) Mousavipour, S. Hosein; Homayoon, Zahra. Multichannel RRKM-TST and CVT Rate Constant Calculations for Reactions of CH_2OH or CH_3O with HO_2. *J. Phys. Chem. A* **2011**, *115* (15), 3291–3300. https://doi.org/10.1021/jp112081r.

(90) Skouteris, Dimitrios; Balucani, Nadia; Ceccarelli, Cecilia; Vazart, Fanny; Puzzarini, Cristina; Barone, Vincenzo; Codella, Claudio; Lefloch, Bertrand. The Genealogical Tree of Ethanol: Gas-Phase Formation of Glycolaldehyde, Acetic Acid, and Formic Acid. *Astrophys. J.* **2018**, *854* (2), 135. https://doi.org/10.3847/1538-4357/aaa41e.

(91) Vichietti, Rafael Mario; Spada, Rene Felipe Keidel; Silva, Albérico Borges Ferreira da; Machado, Francisco Bolivar Correto; Haiduke, Roberto Luiz Andrade. Accurate Calculations of Rate Constants for the Forward and Reverse H_2O + CO ↔ HCOOH Reactions. *ChemistrySelect* **2017**, *2* (24), 7267–7272. https://doi.org/10.1002/slct.201701137.

(92) Yetter, Richard A.; Rabitz, Herschel; Dryer, Frederick L.; Maki, Robert G.; Klemm, R. Bruce. Evaluation of the Rate Constant for the Reaction OH+H_2CO: Application of Modeling and Sensitivity Analysis Techniques for Determination of the Product Branching Ratio. *J. Chem. Phys.* **1989**, *91* (7), 4088–4097. https://doi.org/10.1063/1.456838.

(93) Chang, Jee Gong; Chen, Hsin Tsung; Xu, Shucheng; Lin, M. C. Computational Study on the Kinetics and Mechanisms for the Unimolecular Decomposition of Formic and Oxalic Acids. *J. Phys. Chem. A* **2007**, *111* (29), 6789–6797. https://doi.org/10.1021/jp069036p.

(94) Galano, Annia; Alvarez-Idaboy, J. Raúl; Ruiz-Santoyo, Ma. Esther; Vivier-Bunge, Annik. Rate Coefficient and Mechanism of the Gas Phase OH Hydrogen Abstraction Reaction from Formic Acid: A Quantum Mechanical Approach. *J. Phys. Chem. A* **2002**, *106* (41), 9520–9528. https://doi.org/10.1021/jp020297i.

(95) Glarborg, Peter; Marshall, Paul. The Rate Constant for the CO + H_2O_2 Reaction. *Chem. Phys. Lett.* **2009**, *475* (1–3), 40–43. https://doi.org/10.1016/j.cplett.2009.05.028.

(96) Senosiain, Juan P.; Klippenstein, Stephen J.; Miller, James A. The Reaction of Acetylene with Hydroxyl Radicals. *J. Phys. Chem. A* **2005**, *109* (27), 6045–6055. https://doi.org/10.1021/jp050737g.

(97) Petty, Jeffrey T.; Harrison, John A.; Moore, C. Bradley. Reactions of Trans-Hydroxycarbonyl Radical Studied by Infrared Spectroscopy. *J. Phys. Chem.* **1993**, *97* (43), 11194–11198. https://doi.org/10.1021/j100145a013.

(98) Golden, D. M.; Smith, G. P.; McEwen, A. B.; Yu, C. L.; Eiteneer, B.; Frenklach, M.; Vaghjiani, G. L.; Ravishankara, A. R.; Tully, F. P. OH(OD) + CO: Measurements and an Optimized RRKM Fit. *J. Phys. Chem. A* **1998**, *102* (44), 8598–8606. https://doi.org/10.1021/jp982110m.

(99) Yu, Hua-Gen; Muckerman, James T.; Francisco, Joseph S. Quantum Force Molecular Dynamics Study of the Reaction of O Atoms with HOCO. *J. Chem. Phys.* **2007**, *127* (9), 094302. https://doi.org/10.1063/1.2770463.

(100) Yu, Hua-Gen; Muckerman, James T.; Francisco, Joseph S. Direct Ab Initio Dynamics Study of the OH + HOCO Reaction. *J. Phys. Chem. A* **2005**, *109* (23), 5230–5236. https://doi.org/10.1021/jp051458w.

(101) Larson, C. W.; Stewart, P. H.; Golden, D. M. Pressure and Temperature Dependence of Reactions Proceeding via a Bound Complex. An Approach for Combustion and Atmospheric Chemistry Modelers. Application to HO + CO → [HOCO] → H + CO_2. *Int. J. Chem. Kinet.* **1988**, *20* (1), 27–40. https://doi.org/10.1002/kin.550200105.

(102) Xu, Shucheng; Zhu, R. S.; Lin, M. C. Ab Initio Study of the OH + CH_2O Reaction: The Effect of the OH··OCH_2 Complex on the H-Abstraction Kinetics. *Int. J. Chem. Kinet.* **2006**, *38* (5), 322–326. https://doi.org/10.1002/kin.20166.

(103) Veyret, Bernard; Roussel, Pascal; Lesclaux, Robert. Mechanism of the Chain Process Forming H_2 in the Photooxidation of Formaldehyde. *Int. J. Chem. Kinet.* **1984**, *16* (12), 1599–1608. https://doi.org/10.1002/kin.550161213.

(104) Veyret, Bernard; Rayez, Jean Claude; Lesclaux, Robert. Mechanism of the Photooxidation of Formaldehyde Studied by Flash Photolysis of Formaldehyde-Oxygen-Nitric Oxide Mixtures. *J. Phys. Chem.* **1982**, *86* (17),

3424–3430. https://doi.org/10.1021/j100214a032.

(105) Canosa-mas, C. E.; Frey, H. M.; Walsh, R. Studies of Methylene Chemistry by Pulsed Laser-Induced Decomposition of Ketene. Part 1.—Ketene in the Presence of Noble Gases. *J. Chem. Soc., Faraday Trans. 2* **1984**, *80* (5), 561–578. https://doi.org/10.1039/F29848000561.

(106) Faravelli, T.; Goldaniga, A.; Zappella, L.; Ranzi, E.; Dagaut, P.; Cathonnet, M. An Experimental and Kinetic Modeling Study of Propyne and Allene Oxidation. *Proc. Combust. Inst.* **2000**, *28* (2), 2601–2608. https://doi.org/10.1016/S0082-0784(00)80678-5.

(107) Vandooren, J.; Van Tiggelen, P. J. Reaction Mechanisms of Combustion in Low Pressure Acetylene-Oxygen Flames. *Symp. Combust.* **1977**, *16* (1), 1133–1144. https://doi.org/10.1016/S0082-0784(77)80402-5.

(108) Semenikhin, A. S.; Shubina, E. G.; Savchenkova, A. S.; Chechet, I. V.; Matveev, S. G.; Konnov, A. A.; Mebel, A. M. Mechanism and Rate Constants of the CH_3 + CH_2CO Reaction: A Theoretical Study. *Int. J. Chem. Kinet.* **2018**, *50* (4), 273–284. https://doi.org/10.1002/kin.21156.

(109) Banyard, Stephen A.; Canosa-Mas, Carlos E.; Ellis, Mark D.; Frey, Henry M.; Walsh, Robin. Keten Photochemistry. Some Observations on the Reactions and Reactivity of Triplet Methylene. *J. Chem. Soc. Chem. Commun.* **1980**, No. 23, 1156–1157. https://doi.org/10.1039/c39800001156.

(110) Xiong, Shao Zhuan; Yao, Qian; Li, Ze Rong; Li, Xiang Yuan. Reaction of Ketenyl Radical with Hydroxyl Radical over $C_2H_2O_2$ Potential Energy Surface: A Theoretical Study. *Combust. Flame* **2014**, *161* (4), 885–897. https://doi.org/10.1016/j.combustflame.2013.10.013.

(111) Hassinen, Eero; Kalliorinne, Kaarlo; Koskikallio, Jouko. Kinetics of Reactions between Methyl and Acetyl Radicals in Gas Phase Produced by Flash Photolysis of Acetic Anhydride. *Int. J. Chem. Kinet.* **1990**, *22* (7), 741–745. https://doi.org/10.1002/kin.550220709.

(112) Yasunaga, Kenji; Kubo, Satoshi; Hoshikawa, Hiroki; Kamesawa, Takashi; Hidaka, Yoshiaki. Shock-Tube and Modeling Study of Acetaldehyde Pyrolysis and Oxidation. *Int. J. Chem. Kinet.* **2008**, *40* (2), 73–102. https://doi.org/10.1002/kin.20294.

(113) Wang, Heng; Bozzelli, Joseph W. Thermochemistry and Kinetic Analysis of the Unimolecular Oxiranyl Radical Dissociation Reaction: A Theoretical Study. *ChemPhysChem* **2016**, *17* (13), 1983–1992. https://doi.org/10.1002/cphc.201600152.

(114) Xu, Z. F.; Xu, Kun; Lin, M. C. Thermal Decomposition of Ethanol. 4. Ab Initio Chemical Kinetics for Reactions of H Atoms with CH_3CH_2O and CH_3CHOH Radicals. *J. Phys. Chem. A* **2011**, *115* (15), 3509–3522. https://doi.org/10.1021/jp110580r.

(115) Tsang, Wing. Chemical Kinetic Data Base for Combustion Chemistry. Part 2. Methanol. *J. Phys. Chem. Ref. Data* **1987**, *16* (3), 471–508. https://doi.org/10.1063/1.555802.

(116) Fagerström, Kjell; Lund, Anders; Mahmoud, Gharib; Jodkowski, Jerzy T.; Ratajczak, Emil. Kinetics of the Gas-Phase Reaction between Ethyl and Hydroxyl Radicals. *Chem. Phys. Lett.* **1993**, *208* (3–4), 321–327. https://doi.org/10.1016/0009-2614(93)89083-T.

(117) Heicklen, Julian. The Decomposition of Alkyl Nitrites and the Reactions of Alkoxyl Radicals. In *Advances in Photochemistry*; 1988; Vol. 14, pp 177–272. https://doi.org/10.1002/9780470133446.ch4.

(118) Aders, W. K.; Wagner, H. Gg. Untersuchungen Zur Reaktion von Wasserstoffatomen Mit Äthanol Und Tert. Butanol. *Berichte der Bunsengesellschaft für Phys. Chemie* **1973**, *77* (9), 712–718. https://doi.org/10.1002/bbpc.19730770911.

(119) Olm, Carsten; Varga, Tamás; Valkó, Éva; Hartl, Sandra; Hasse, Christian; Turányi, Tamás. Development of an Ethanol Combustion Mechanism Based on a Hierarchical Optimization Approach. *Int. J. Chem. Kinet.* **2016**, *48* (8), 423–441. https://doi.org/10.1002/kin.20998.

(120) Li, Juan; Kazakov, Andrei; Dryer, Frederick L. Experimental and Numerical Studies of Ethanol Decomposition Reactions. *J. Phys. Chem. A* **2004**, *108* (38), 7671–7680. https://doi.org/10.1021/jp0480302.

(121) Tsang, Wing. Energy Transfer Effects during the Multichannel Decomposition of Ethanol. *Int. J. Chem. Kinet.* **2004**, *36* (8), 456–465. https://doi.org/10.1002/kin.20015.

(122) Kato, A.; Cvetanović, R. J. Reaction of Oxygen Atoms with Ethanol. *Can. J. Chem.* **1967**, *45* (16), 1845–1861. https://doi.org/10.1139/v67-297.

(123) Noell, A. C.; Alconcel, L. S.; Robichaud, D. J.; Okumura, M.; Sander, S. P. Near-Infrared Kinetic Spectroscopy of the HO_2 and $C_2H_5O_2$ Self-Reactions and Cross Reactions. *J. Phys. Chem. A* **2010**, *114* (26), 6983–6995. https://doi.org/10.1021/jp912129j.

(124) Bozzelli, Joseph W.; Dean, Anthony M. Chemical Activation Analysis of the Reaction of Ethyl Radical with Oxygen. *J. Phys. Chem.* **1990**, *94* (8), 3313–3317. https://doi.org/10.1021/j100371a021.

(125) Denisov, E. T. Mechanisms of the Reactions of Radicals with Ozone. *Russ. J. Phys. Chem. B* **2008**, *2* (1), 58–66. https://doi.org/10.1134/S1990793108010090.

(126) Zhang, Pei; Wang, Wenliang; Zhang, Tianlei; Chen, Long; Du, Yongmei; Li, Chunying; Lü, Jian. Theoretical Study on the Mechanism and Kinetics for the Self-Reaction of $C_2H_5O_2$ Radicals. *J. Phys. Chem. A* **2012**, *116* (18), 4610–4620. https://doi.org/10.1021/jp301308u.

(127) Sheng, Chad Y.; Bozzelli, Joseph W.; Dean, Anthony M.; Chang, Albert Y. Detailed Kinetics and Thermochemistry of $C_2H_5 + O_2$: Reaction Kinetics of the Chemically-Activated and Stabilized CH_3CH_2OO• Adduct. *J. Phys. Chem. A* **2002**, *106* (32), 7276–7293. https://doi.org/10.1021/jp014540+.

(128) Harding, Lawrence B.; Klippenstein, Stephen J.; Georgievskii, Yuri. Reactions of Oxygen Atoms with Hydrocarbon Radicals: A Priori Kinetic Predictions for the CH_3+O, C_2H_5+O, and C_2H_3+O Reactions. *Proc. Combust. Inst.* **2005**, *30* (1), 985–993. https://doi.org/10.1016/j.proci.2004.08.184.

(129) Atkinson, R.; Finlayson, B. J.; Pitts, J. N. Photoionization Mass Spectrometer Studies of Gas Phase Ozone-Olefin Reactions. *J. Am. Chem. Soc.* **1973**, *95* (23), 7592–7599. https://doi.org/10.1021/ja00804a008.

(130) Atkinson, R.; Baulch, D. L.; Cox, R. A.; Crowley, J. N.; Hampson, R. F.; Hynes, R. G.; Jenkin, M. E.; Rossi, M. J.; Troe, J.; Subcommittee, IUPAC. Evaluated Kinetic and Photochemical Data for Atmospheric Chemistry: Volume II – Gas Phase Reactions of Organic Species. *Atmos. Chem. Phys.* **2006**, *6* (11), 3625–4055. https://doi.org/https://doi.org/10.5194/acp-6-3625-2006.

(131) Edelbüttel-Einhaus, Jürgen; Hoyermann, Karlheinz; Rohde, Gabriele; Seeba, Johann. The Detection of the Hydroxyethyl Radical by Rempi/Mass-Spectrometry and the Application to the Study of the Reactions CH_3CHOH+O and CH_3CHOH+H. *Symp. Combust.* **1992**, *24* (1), 661–668. https://doi.org/10.1016/S0082-0784(06)80081-0.

(132) Xu, Zhen Feng; Xu, Kun; Lin, Ming Chang. Ab Initio Kinetics for Decomposition/Isomerization Reactions of C_2H_5O Radicals. *ChemPhysChem* **2009**, *10* (6), 972–982. https://doi.org/10.1002/cphc.200800719.

(133) Zhang, Yue; Zhang, Shaowen; Li, Qian Shu. Ab Initio Calculations and Mechanism of Two Proton Migration Reactions of Ethoxy Radical. *Chem. Phys.* **2005**, *308* (1–2), 109–116. https://doi.org/10.1016/j.chemphys.2004.08.004.

(134) da Silva, Gabriel; Bozzelli, Joseph W. Role of the α-Hydroxyethylperoxy Radical in the Reactions of Acetaldehyde and Vinyl Alcohol with HO_2. *Chem. Phys. Lett.* **2009**, *483* (1–3), 25–29. https://doi.org/10.1016/j.cplett.2009.10.045.

(135) Atkinson, R.; Baulch, D. L.; Cox, R. A.; Hampson, R. F.; Kerr, J. A.; Rossi, M. J.; Troe, J. Evaluated Kinetic and Photochemical Data for Atmospheric Chemistry, Organic Species: Supplement VII. *J. Phys. Chem. Ref. Data* **1999**, *28* (2), 191–393. https://doi.org/10.1063/1.556048.

(136) Galano, Annia; Alvarez-Idaboy, J. Raúl; Bravo-Pérez, Graciela; Ruiz-Santoyo, Ma Esther. Gas Phase Reactions of C_1 –C_4 Alcohols with the OH Radical: A Quantum Mechanical Approach. *Phys. Chem. Chem. Phys.* **2002**, *4* (19), 4648–4662. https://doi.org/10.1039/B205630E.

(137) Rosado-Reyes, Claudette; Tsang, Wing. Bond Cleavage During Isobutanol Thermal Decomposition and the Breaking of C–C Bonds in Alcohols at High Temperatures. *J. Phys. Chem. A* **2013**, *117* (40), 10170–10177. https://doi.org/10.1021/jp404877t.

(138) Pokidova, T. S.; Denisov, E. T.; Shestakov, A. F. Kinetic Parameters and Geometry of the Transition State in the Unimolecular Degradation of Alcohols. *Pet. Chem.* **2009**, *49* (5), 343–353. https://doi.org/10.1134/S0965544109050016.

(139) Goldsmith, C. Franklin; Green, William H.; Klippenstein, Stephen J. Role of O_2 + QOOH in Low-Temperature Ignition of Propane. 1. Temperature and Pressure Dependent Rate Coefficients. *J. Phys. Chem. A* **2012**, *116* (13), 3325–3346. https://doi.org/10.1021/jp210722w.

(140) Villano, Stephanie M.; Carstensen, Hans-Heinrich; Dean, Anthony M. Rate Rules, Branching Ratios, and Pressure Dependence of the HO_2 + Olefin Addition Channels. *J. Phys. Chem. A* **2013**, *117* (30), 6458–6473. https://doi.org/10.1021/jp405262r.

(141) Huang, Haifeng; Merthe, Daniel J.; Zádor, Judit; Jusinski, Leonard E.; Taatjes, Craig A. New Experiments and Validated Master-Equation Modeling for OH Production in Propyl+O_2 Reactions. *Proc. Combust. Inst.* **2011**, *33* (1), 293–299. https://doi.org/10.1016/j.proci.2010.06.039.

(142) Kerr, J. A.; Lloyd, A. C. Kinetics and Pressure Dependence of the Decomposition of the Propionyl Radical. *Trans. Faraday Soc.* **1967**, *63* (7), 2480–2488. https://doi.org/10.1039/tf9676302480.

(143) Wagner, Albert F.; Slagle, Irene R.; Sarzynski, Dariusz; Gutman, David. Experimental and Theoretical Studies of the Ethyl + Oxygen Reaction Kinetics. *J. Phys. Chem.* **1990**, *94* (5), 1853–1868. https://doi.org/10.1021/j100368a026.

(144) Baker, R. R.; Baldwin, R. R.; Walker, R. W. The Use of the H_2+O_2 Reaction in Determining the Velocity Constants of Elementary Reaction in Hydrocarbon Oxidation. *Symp. Combust.* **1971**, *13* (1), 291–299. https://doi.org/10.1016/S0082-0784(71)80032-2.

(145) Singleton, D. L.; Irwin, R. S.; Cvetanović, R. J. Arrhenius Parameters for the Reactions of O(3P) Atoms with Several Aldehydes and the Trend in Aldehydic C—H Bond Dissociation Energies. *Can. J. Chem.* **1977**, *55* (18), 3321–3327. https://doi.org/10.1139/v77-463.

(146) Dixon, David J.; Skirrow, Geoffrey; Tipper, Charles F. H. Low Temperature Gas-Phase Oxidation of Aldehydes. Part 1.—The Reaction below 120°C. *J. Chem. Soc. Faraday Trans. 1 Phys. Chem. Condens. Phases* **1974**, *70*, 1078–1089. https://doi.org/10.1039/f19747001078.

(147) Zügner, Gábor L.; Szilágyi, István; Zádor, Judit; Szabó, Emese; Dóbé, Sándor; Song, Xinli; Wang, Baoshan. OH Yields for $C_2H_5CO+O_2$ at Low Pressure: Experiment and Theory. *Chem. Phys. Lett.* **2010**, *495* (4–6), 179–181. https://doi.org/10.1016/j.cplett.2010.06.089.

(148) Baldwin, R. R.; Lewis, K. A.; Walker, R. W. Carbon Dioxide Formation in Oxidation of Propionaldehyde. *Combust. Flame* **1979**, *34*, 275–283. https://doi.org/10.1016/0010-2180(79)90102-0.

(149) Peter, A.; Acs, G.; Horvath, I.; Huhn, P. Decomposition of Propionaldehyde Initiated by the Thermal Decomposition of Azoethane. *Acta Chim. Hung.* **1981**, *108*.

(150) McElroy, D.; Walsh, C.; Markwick, A. J.; Cordiner, M. A.; Smith, K.; Millar, T. J. The UMIST Database for Astrochemistry 2012. *Astron. Astrophys.* **2013**, *550*, A36. https://doi.org/10.1051/0004-6361/201220465.

(151) Geppert, Wolf D.; Thomas, Richard; Ehlerding, Anneli; Semaniak, Jacek; Österdahl, Fabian; Ugglas, Magnus Af; Djurić, Nada; Paál, András; Larsson, Mats. Extraordinary Branching Ratios in Astrophysically Important Dissociative Recombination Reactions. *Faraday Discuss.* **2004**, *127*, 425–437. https://doi.org/10.1039/b314005a.

(152) Ganguli, B.; Biondi, M. A.; Johnsen, R.; Dulaney, J. L. Electron-Temperature Dependence of the Recombination of HCO^+ Ions with Electrons. *Phys. Rev. A* **1988**, *37* (7), 2543–2547. https://doi.org/10.1103/PhysRevA.37.2543.